Estimates of lightning NOx production from GOME satellite observations

K. F. Boersma, H. J. Eskes, E. W. Meijer, H. M. Kelder

Atmos. Chem. Phys. Discuss., 5, 3047–3104, 2005
www.atmos-chem-phys.org/acpd/5/3047/
SRef-ID: 1680-7375/acpd/2005-5-3047
European Geosciences Union

Atmospheric Chemistry and Physics Discussions

Estimates of lightning NO_x production from GOME satellite observations

K. F. Boersma, H. J. Eskes, E. W. Meijer, and H. M. Kelder

Royal Netherlands Meteorological Institute, De Bilt, The Netherlands

Received: 17 February 2005 – Accepted: 4 April 2005 – Published: 13 May 2005

Correspondence to: K. F. Boersma (boersma@knmi.nl)

Abstract

Tropospheric NO_2 column retrievals from the Global Ozone Monitoring Experiment (GOME) satellite spectrometer are used to quantify the source strength and 3D distribution of lightning produced nitrogen oxides (NO_x=NO_2+NO_2). A sharp increase of NO_2 is observed at convective cloud tops with increasing cloud top height, consistent with a power-law behaviour with power 5±2. Convective production of clouds with the same cloud height are found to produce NO_2 with a ratio 1.6/1 for continents compared to oceans. This relation between cloud properties and NO_2 is used to construct a 10:30 local time global lightning NO_2 production map for 1997. An extensive statistical comparison is conducted to investigate the capability of the TM3 chemistry transport model to reproduce observed patterns of lightning NO_2 in time and space. This comparison uses the averaging kernel to relate modelled profiles of NO_2 to observed NO_2 columns. It exploits a masking scheme to minimise the interference of other NO_x sources on the observed total columns. Simulations are performed with two lightning parametrisations, one relating convective preciptation (CP scheme) to lightning flash distributions, and the other relating the fifth power of the cloud top height (H5 scheme) to lightning distributions. The satellite-retrieved NO_2 fields show significant correlations with the simulated lightning contribution to the NO_2 concentrations for both parametrisations. Over tropical continents modelled lightning NO_2 shows remarkable quantitative agreement with observations. Over the oceans however, the two model lightning parametrisations overestimate the retrieved NO_2 attributed to lightning. Possible explanations for these overestimations are discussed. The ratio between satellite-retrieved NO_2 and modelled lightning NO_2 is used to rescale the original modelled lightning NO_x production. Eight estimates of the lightning NO_x production in 1997 are obtained from spatial and temporal correlation methods, from cloud-free and cloud-covered observations, and from two different lightning parametrisations. Accounting for a wide variety of random and possible systematic errors, we estimate the global NO_x production from lightning to be in the range 1.1–6.4 TgN in 1997.

ACPD

5, 3047–3104, 2005

1. Introduction

Lightning produces substantial amounts of atmospheric nitrogen oxides (NO_x=NO+NO_2), key species that control the formation of tropospheric ozone (e.g. Crutzen, 1970) and influence the oxidising capacity of the troposphere (e.g. Labrador et al., 2004a). However, recent estimates of the annual global lightning NO_x production range from 0.9 to 13.2 TgN, and the reported uncertainties of individual estimates have comparable magnitudes (see Table 1 for an overview). The ozone budget in the upper troposphere (UT) is strongly influenced by NO_x and reliable estimates of the global lightning-produced NO_x (hereafter LNOx) budget are important for accurate knowledge of ozone in the UT where it is an efficient greenhouse gas. Appropriate quantification of the LNOx budget is also important for estimating the lifetime of long-lived greenhouse gases such as methane, whose lifetime is determined by the OH concentration. Furthermore, the current level of uncertainty in LNOx is hampering quantitative assessments of NO_x concentrations resulting from emissions by other sources such as industry and transport, biomass burning, soils and aircraft (Olivier et al., 2001).

Most estimates of the annual LNOx budget published so far (Table 1) have modelled LNOx in a "bottom-up" way. Bottom-up methods generally count the number of lightning flashes and make assumptions on lightning characteristics – like NO_x production efficiency per flash, energy ratio of cloud-to-ground (CG) to intra-cloud (IC) flashes – with only limited observational constraints (e.g. Nesbitt et al., 2000; Price et al., 1997a) to estimate the total LNOx production. Until recently there was lack of space observations and fundamental difficulties exist in extrapolating local in-situ (Levy et al., 1996) or regional (Beirle et al., 2004) observations to the global scale. Satellite measurements have the potential to solve this issue since global tropospheric columns of NO_2 from GOME have become available (e.g. Leue et al., 2001; Richter and Burrows, 2002; Martin et al., 2002; Boersma et al., 2004). Measurements by GOME are sensitive to tracers residing in the middle and upper troposphere such as NO_x from lightning. However, the

ACPD
5, 3047–3104, 2005

LNOx contribution to the total observed column is at most 10%, which severely complicates the discrimination of the lightning contribution from other tropospheric sources, the stratospheric background, and the measurement noise.

Several examples of enhanced NO_2 near thunderstorm complexes have been reported based on the GOME observations (e.g. Choi et al., 2005). Beirle et al. (2004) found a good correlation between monthly mean satellite measurements of tropospheric NO_2 columns and monthly mean lightning flash distributions measured by the Lightning Image Sensor (LIS) over Australia. Hild et al. (2002) demonstrated that GOME is sensitive to LNOx deposited in a thunderstorm cloud. Apart from information on trace gases, GOME spectra also contain information on cloud fraction and cloud top altitude which is crucial for the LNOx study. In this paper we will extend the individual observations by presenting a statistical study of NO_x enhancements at high clouds, based on the FRESCO cloud retrieval scheme (Koelemeijer et al., 2001).

Furthermore, we reverse in this work the often used "bottom-up" approach to determine the annual LNOx production by imposing constraints on distributions of modelled lightning NO_2 (herafter LNO2) in the tropics by satellite observations. Levy et al. (1996) compared tropospheric NO_x simulations with aircraft measurements of LNOx over various isolated regions in the world. While their comparisons were necessarily based on a limited number of aircraft flights, we present an extensive statistical study of LNOx based on a full year (1997) of contiguous tropical GOME observations. We focus on situations downwind of storm systems over areas relatively free from pollution to avoid (1) difficulties related to large contributions from urban and biomass burning NO_x emissions, (2) complexities related to the radiative transport and profile shape dependency over thunderstorm situations (Hild et al., 2002), and partly also to avoid (3) difficulties in extrapolating the 10:30 local time measurements to values representative for the whole day. Because of the large data set available we arrive at significant results despite the small signal to noise ratio.

This paper is organised as follows: Sect. 2 describes the GOME tropospheric NO_2 observations, and Sect. 3 gives observational evidence that GOME detects strongly

enhanced LNO2 in situations where high clouds are present. Section 4 describes a statistical method for the comparison of modelled LNO2 and observed patterns of (lightning) NO_2 columns, the way to correct for interfering NO_x from other sources, and is followed by a discussion of the results. Section 5 shows annual mean modelled and GOME-derived LNO2 distributions. In Sect. 6, we use the ratio between modelled and observed LNO2 to provide a top-down estimate of the global LNOx production in 1997, and discuss the various sources of error in our method.

2. GOME tropospheric NO_2 observations

In this study we use tropospheric NO_2 columns determined with the retrieval-assimilation-modelling approach as developed during the European Union GOA project. The retrieval is based on a set of slant column densities retrieved by the University of Heidelberg (Wagner et al., 1999; Wenig et al., 2004). These columns are assimilated with the TM3 chemistry-transport model. The analysed stratospheric NO_x model field obtained in this way is consistent with both the GOME observations and analysed stratospheric dynamics from the European Centre for Medium-Range Weather Forecasts (ECMWF) used to drive the model. A tropospheric air mass factor is used to convert the tropospheric slant column density (total slant column – assimilated 'stratospheric' slant column) into a tropospheric vertical column density. Radiative transfer modelling for air mass factor calculation accounts for viewing geometry, cloud coverage and cloud top pressure, surface albedo and a priori NO_2 profile shapes modelled with TM3 for the GOME pixel position and time. Cloud information is retrieved from the FRESCO algorithm (Koelemeijer et al., 2001) that uses the strength of the absorption in the O_2–A band (758–778 nm) to estimate an effective cloud top height. The effective cloud top altitude is a measure for how far light penetrated into the atmosphere. Because of penetration of the light into the cloud this effective altitude typically corresponds to a level below the physical cloud top. The 'continuum' reflectance level around the O_2–A band is used to determine the cloud fraction. More details on the tropospheric NO_2 retrieval

ACPD
5, 3047–3104, 2005

can be found in Boersma et al. (2004).

There are four important features that make these retrievals especially suitable for the LNOx study: (1) The correction for the stratospheric background is performed with an assimilation approach that explicitly accounts for zonal variability in the stratospheric NO_2 column caused by stratospheric dynamics, (2) A detailed error propagation is carried out for each individual retrieval (Boersma et al., 2004). This fully accounts for all error sources in the retrieval method (i.e., errors in the slant column fitting, in estimating stratospheric NO_2, and errors in cloud and albedo information), (3) The averaging kernel (AK) (Eskes and Boersma, 2003) that is associated with every individual retrieval is part of the data product. The AK allows model-predicted profiles to be compared directly to satellite retrieved columns by removing the comparison's dependence on the a priori assumed profile shape. The averaging kernels also allows a meaningful model-GOME comparison in cases of full or partial cloud cover. (4) Explicit information of cloud fraction and cloud top altitude is retrieved based on the FRESCO algorithm (Koelemeijer et al., 2001).

Up till now, there is little independent NO_2 profile data available to validate the tropospheric column retrievals. Also, nitrogen oxides in the boundary layer have a large spatial and temporal variability. A comparison with in situ aircraft observations reported by Martin et al. (2004) shows that, on average, uncollocated in situ aircraft measurements of tropospheric NO_2 are consistent with GOME retrievals as described by Martin et al. (2002). An extensive set of surface NO_2 measurements is available on a routine basis from operational networks in Europe and America. However, in order to relate these surface concentrations to the retrieved column abundances, additional information is needed on the vertical distribution of NO_x. A recent study by Blond et al. (2005)[1] shows good quantitative agreement of yearly-mean values and spatial patterns over

[1] Blond, N., Boersma, K. F., Eskes, H. J., van der A, R., Van Roozendael, M., De Smedt, I., Bergametti, G., and Vautard, R.: Intercomparison of SCIAMACHY nitrogen dioxide observations, in-situ measurements and air quality modeling results over Western Europe, J. Geophys. Res., submitted, 2005.

Europe from measured and modelled (CHIMERE) surface concentrations of NO_2, as well as between modelled and retrieved (SCIAMACHY) columns of NO_2. These SCIAMACHY columns have been retrieved with the same approach as used in this work.

Aircraft measurements have shown that a large fraction of the LNOx is deposited in the UT and upper part of clouds (e.g. Ridley et al., 1994; Pickering et al., 1998). Figure 1 in Eskes and Boersma (2003) shows that even for scenes completely free of clouds the sensitivity to UT NO_2 is only slightly below typical stratospheric sensitivities. The situation for cloudy scenes is more complex as clouds can both increase and decrease the capability of GOME to detect a tropospheric NO_2 signal. Clouds below a NO_2 layer increase the effective albedo of the scene, thereby increasing the detected slant column. On the other hand, high clouds may (partly) screen the NO_2 column below, thereby decreasing the signal. The higher the cloud fraction the stronger the effects described above. Figure 1 illustrates the effects for a scenario in terms of cloud height, cloud fraction, the Tracer Model 3 (TM3, Dentener et al., 2003) predicted vertical NO_2 profile shape, and the corresponding averaging kernel (Eskes and Boersma, 2003). The two panels in Fig. 1 serve as an example of a scene with a high effective cloud top altitude (≈750 hPa) and a cloud fraction of 0.26. The surface albedo was 0.05, solar zenith angle 5.8°, and viewing zenith angle 26.0° for this scene. The right panel shows the high sensitivity of GOME for NO_2 above the cloud. Note that NO_2 may be present just above 750 hPa, while NO_2 below the cloud top is effectively invisible for GOME.

The uncertainties for individual GOME measurements (Boersma et al., 2004) in the Southern Hemisphere tropics are shown in Fig. 2. For retrieved columns with small values, the uncertainty is dominated by the combined error from the spectral fitting and from the stratospheric column estimate. For columns exceeding $0.5{\cdot}10^{15}$ molec.cm^{-2}, the uncertainty grows due to increasing errors related to cloud fraction, albedo and profile shape. In this study, 95% of the encountered columns are in the $[-0.7, +1.0]\times10^{15}$ molec.cm^{-2} range and corresponding retrieval errors for individual GOME pixels are in the $[0.3–0.6]\times10^{15}$ molec.cm^{-2} range.

3. Detection of LNO2

In this section we investigate the dependence of LNOx production on cloud height, based on the cloud properties and NO_2 columns retrieved from the GOME observations. High clouds are known to be related to enhanced lightning activity and enhanced NO_x production. Price and Rind (1992) argue that the lightning activity is correlated with cloud top height, since both are largely determined by the updraft intensity. For a range of simultaneous lightning and cloud top height observations, they derived a relationship where lightning activity is proportional to the fifth power of the storm dimension – or cloud top – H, i.e. higher clouds are expected to have strong increases in lightning activity. Ushio et al. (2001) also found an exponential increase in satellite-observed lightning intensity as a function of satellite-observed cloud height.

Figure 3 schematically describes the retrieval approach when clouds are present: the left part shows how photons sample the upper parts of the cloud before they are scattered back, and the right part shows the simplified representation of cloud scattering in our cloud scheme. In the FRESCO cloud retrieval, a cloud is approximated as a Lambertian reflecting surface with an albedo of 0.8 and the effective cloud top height corresponds to the height the surface needs to be lifted in a radiative transfer model to best match the measured depth of the O_2–A band. This effective cloud top height is depicted as the lowest dotted line in the left panel of Fig. 3. The same Lambertian reflector model is used in the radiative transfer calculations for the NO_2 retrievals.

In situations of high clouds with strong lightning activity, a large fraction of the LNOx ends up in the top and anvil (Ridley et al., 1996) of the cloud where GOME has an enhanced sensitivity to LNOx. A radiative-transfer study by Hild et al. (2002) shows that even in the case of thick clouds GOME is able to detect NO_x present several kilometers below the cloud top, consistent with our own calculations. One source of error in the cloud height is the fact that the FRESCO cloud top height is retrieved from photons with wavelengths near 758–778 nm, and may be different from the penetration depth (effective cloud top height) of photons with wavelengths near 440 nm used in

ACPD
5, 3047–3104, 2005

the NO_2 retrieval procedure. Nevertheless, we expect that this error is small as cloud particles have scattering characteristics that hardly depend on wavelength in the visible part of the spectrum.

For our study of the dependence of observed NO_2 columns on cloud height for cloudy scenes, we used GOME observations over tropical oceans and continents in the 40° S–5° N area. This area is characterised by strong lightning activity and the influence of other sources of NO_x (see Sect. 4) is relatively minor. We consider the subset of GOME observations where the reflectance of the cloud-covered part of the scene exceeds 75% of the total measured reflectance. To avoid ghost column difficulties, the "above-cloud" part of the NO_2 column is retrieved by discarding the model predicted ghost column in the air mass factor ($M'_{tr}=N_s/N'_v$) calculation, with the corrected vertical column N'_v defined as:

$$N'_v = w \cdot (N_v - N_{v,ghost}) + (1 - w) \cdot N_v, \quad (1)$$

with N_v the total predicted vertical column (that is normally used in air mass factor calculations), $N_{v,ghost}$ the ghost column from the surface up to the effective cloud height, and w the cloud reflectance fraction. Note that the satellite thus measures the integral of NO_2 concentrations from the cloud top to the tropopause. All tropospheric above-cloud NO_2 columns were stored in 5 hPa cloud top pressure bins. The annual mean tropospheric NO_2 column was calculated only if there were more than 15 measurements in a bin.

The upper panel of Fig. 4 shows the annual mean tropospheric NO_2 columns over tropical oceans as a function of cloud top height and the lower panel shows the same for tropical continents. The insets in both panels show a log-log plot of the same curve for cloud top pressures below 440 hPa (above circa 6.5 km). Clouds with tops below 6.5 km are assumed not to produce substantial amounts of lightning. The increase relative to a background – resulting from other sources of NO_2 – is consistent with a power law (see insets). The solid line is a fit of the form $A + BH^C$ with H the cloud top height, A, B free coefficients and a power C=4.6 for tropical oceans, and C=5.1

for tropical continents. This power however is quite sensitive to assumptions about the (height-dependence of the) background, or coefficient A. From fits with different choices of A we arrive at a conservative error estimate on C of ±2 for both tropical oceans and continents (Ushio et al., 2001). The dependence of the observed NO_2 on cloud height is surprisingly consistent with the power-law parametrisation of LNOx in CTMs (Price and Rind, 1992). However, the power-law relation that we found is one of many functions that may fit the increase of NO_2 with cloud height well, and this result should not be interpreted as a validation of of the power-law parametrisation of Price and Rind (1992).

Often, the optical thickness of clouds is proportional to their geometrical thickness (Feigelson, 1984), so multiple scattering effects may change with cloud height. However, Hild et al. (2002) found that the air mass factor is hardly dependent on the cloud particle densities typical for thunderstorm clouds. We observe a very sharp and large increase of tropospheric NO_2 for clouds higher than 10 km. It is unlikely that this observed sharp increase would be the result of a strong change in cloud properties with altitude.

The results in Fig. 4 allow us to derive a ratio of LNOx production efficiencies of clouds over land and sea respectively. Fixing the power law coefficient C to 4.9 – a choice which is allowed within the error bars – we find that the production in terms of lightning NO_2 column density ($\times 10^{15}$ molec.cm^{-2}) over continents equals $4.75 \cdot 10^{-6} H^{4.9}$, and over oceans $2.98 \cdot 10^{-6} H^{4.9}$. On average, we find that clouds of equal height produce (4.75/2.98=) 1.6 times more LNO2 over continents than over oceans at 10:30 hrs local time (the overpass time of GOME). This ratio is not sensitive to details of our calculation (choice of background or difference between exponents), but is a direct measurement result. The size of the increase observed over high clouds is quite similar in absolute amount. For comparison, in TM3 a 24-h average ratio of 10 (Levy et al., 1996; Christian et al., 2003) is used, whereas for instance Michalon et al. (1999) derive a 24-average ratio of 5. Mesoscale convective systems over continents have a distinct minimum in convective activity at approximately 10:30 h and a strong

maximum in the late afternoon whereas the diurnal cycle over the oceans is much weaker (Nesbitt and Zipser, 2002). Hence a ratio of 1.6 is most likely at the lower end of the 24-h cycle of convective intensity ratios.

The relation between cloud top height and LNOx production allows us to produce a map of the global distribution of the 1997 average LNO2 production at 10:30 h. Application of the LNO2 production parametrisations over continents ($4.75{\cdot}10^{-6}H^{4.9}$) and over oceans ($2.98{\cdot}10^{-6}H^{4.9}$) to all available FRESCO cloud height (H) data in 1997 results in Fig. 5. The most striking feature in Fig. 5 is the large average production of LNO2 over tropical oceans relative to the small production over tropical continents. The observed patterns in Fig. 5 are representative for a 10:30 h local time snapshot of convective activity: little convective activity and hence little lightning over continents is opposed to considerable activity over the tropical oceans.

Deriving quantitative NO_2 estimates from the observed cloud height dependence is difficult. The visible light detected by GOME samples only part of the cloud and the column above the cloud, as shown in Fig. 3. Quantitative estimates of the NO_2 column depend on assumed LNOx profiles inside the cloud and cloud anvil, and on details of the light paths in the inhomogeneous cloud cover inside the large GOME footprint of $40{\times}320\,km^2$. Moreover, a meaningful quantitative estimate of the NO_2 production requires scaling of the 10:30 h local time observed production to values representative for 24-h averages. Also the large footprint of GOME of $320{\times}40\,km^2$ as compared to typical sizes of convective cloud complexes complicates the interpretation of the results. Nevertheless, the rapid increase in observed NO_2 for high clouds strongly suggests that GOME is indeed capable of detecting LNOx production.

4. Statistical comparison of observed NO_2 and modelled LNO2

Apart from investigating above-cloud NO_2 columns as a function of cloud height, additional information on the NO_2 from lightning may be obtained from a comparison of modelled LNO2 and observed NO_2 columns. We compare space and time-dependent

patterns of observed NO_2 with modelled LNO2 downwind of thunderstorms. First, the model and lightning parametrisations are introduced. Then, the comparison method is explained, followed by an introduction on a correction for the influence of NO_x from other sources. The section concludes with the results of the comparison and an interpretation of the results.

4.1. TM3 model and lightning parametrisations

The TM3 model, driven by 6-hourly meteorological analyses of the European Centre for Medium-Range Weather Forecasts (ECMWF), is a 3-D global chemistry-transport model that evaluates the NO_2 production by lightning and subsequent transport, chemical conversion, and the removal of NO_2 from the atmosphere. The model simulations are performed with a spatial resolution of 144×72 grid cells (2.5°×2.5°) and 31σ hybrid-pressure levels from the surface up to 10 hPa. Recently the performance of TM3 was evaluated by comparing model simulations with aircraft observations from various aircraft campaigns (Meijer et al., 2000; Brunner et al., 2003, 2005).

TM3 has two parametrisations available for the calculation of lightning flashes and subsequent NO_x production, one based on convective precipitation (Meijer et al., 2001) (CP) and one based on a power-law (H5) parametrisation (Price and Rind, 1992). Both schemes are described in more detail below.

4.1.1. Convective precipitation scheme

The CP scheme is motivated by the observed good correlation between convective precipitation and the number of lightning flashes (Meijer et al., 2001) over summertime Central Europe. Analysis of the National Lightning Detection Network (NLDN) data of the United States by Brunner and Van Velthoven (1999) also indicates a linear relationship of lightning with convective precipitation. Moreover the CP scheme showed good results between modelled NO_x concentrations and aircraft observations for situations downwind of thunderstorms (Meijer et al., 2001). To account for differences

in convective regimes between continents and oceans, the CP scheme follows the recommendation by Levy et al. (1996) that deep convection over oceans is 10 times less efficient in generating lightning than deep moist convection over continents, due to much weaker vertical velocities in tropical clouds over oceans than over continents. The fraction of CG to the total number of flashes (CG + intra-cloud (IC)) is determined by a 4th order polynomial fit of the thickness of the (ECMWF) cloud above 0°C as proposed by Price and Rind (1993). CG strokes are assumed to be 10 times more energetic than IC strokes following Price et al. (1997a). The production efficiency of NO_x by lightning is set by constraining the global annual LNOx to 5 TgN for the reference year 1998, a number recommended by Lee et al. (1997) and commonly applied in CTM studies. Due to meteorological variations, the net production of NO_x from lightning may be slightly different from 5 TgN in other years, as the scale factor of the reference year (1998) remains constant. For the year 1997, the total emission by lightning amounts to 5.65 TgN, of which 91% occurs between 30° S and 30° N. The lightning NO_x is distributed vertically following lightning NO_x profile shapes obtained by Pickering et al. (1998). These profiles are scaled to cloud top heights in TM3 with the following specifications: (1) all IC NO_x and 70% of CG NO_x is placed between T=−15°C and cloud top, (2) 10% of CG NO_x is placed between the Earth's surface and T=−15°C, and (3) 20% of CG NO_x is placed in the boundary layer. Subsequently, the lightning NO_x within a model layer is distributed proportional to the mass of each layer.

4.1.2. H5 scheme

The H5 scheme is based on the observed relation between the lightning activity and approximately the fifth power of the storm cloud height H. There is additional observational evidence for the validity of applying a fifth power law to cloud top heights from Ushio et al. (2001), with a reported uncertainty of ±2 on the power 5 number. In TM3 maximum altitudes of convective transport are used as measure for the storm dimension H. Apart from the spatial and temporal distribution of the lightning flashes, all other specifications are identical to those in the CP scheme. An important deviation from the

'standard' H5 scheme is that the distribution of flashes for marine clouds ($\sim H^{1.73}$) is replaced by the distribution of flashes for continental convective clouds ($\sim H^{4.9}$) scaled with 0.1, a factor that supposedly corrects for weaker convection over sea (Levy et al., 1996). For 1997, the total nitrogen lightning emissions is 6.4 TgNyr^{-1}, of which 86% between 30° S and 30° N.

4.2. Comparison method

Analysed meteorological fields represent a reconstruction of the actual meteorological state based on observations. The lightning schemes are driven by cloud parameters taken from the ECMWF analyses, which enables TM3 to position the LNOx production at the actual locations and times of convective activity. Modelled LNO2 profiles are simulated by taking the difference of two TM3 model runs, one run with the lightning parametrisation included, and one run with lightning excluded. LNO2 profiles are interpolated in time and space to the location of the GOME pixel.

4.2.1. Averaging kernels

In order to compare modelled NO_2 with the GOME tropospheric column observations we compute a modelled GOME-equivalent tropospheric column $\hat{x}_{LNO_2}$ based on the model LNO2 profile $\boldsymbol{x}_{\boldsymbol{LNO_2}}$ and the averaging kernel $\boldsymbol{A}$:

$$\hat{x}_{LNO_2} = \boldsymbol{A} \cdot \boldsymbol{x}_{\boldsymbol{LNO_2}}. \quad (2)$$

The advantage of a comparison through the kernel is that the comparison is now independent of the a priori profile shape chosen in the retrieval (Eskes and Boersma, 2003) and that cloud-covered pixels can be compared more realistically. The contributions to the (forward model parameter) error in the comparison now only originate from errors in the slant column and representativeness errors in the altitude-dependent air mass factor (see Boersma et al., 2004).

4.2.2. Masking NO_x source areas

Note that, contrary to the modelled pure lightning NO_2 column, the observed column comprises contributions of LNO2 but also from contributions by biomass burning, urban, and soil NO_x emissions. Therefore we apply a masking scheme to exclude areas with known urban and biomass burning emissions. First the highly industrialised Northern Hemisphere is ruled out, leaving the six tropical regions defined in Fig. 10. These regions are subject to additional masking using the DMSP Optical Linescan System (OLS) global nighttime lights climatology (Elvidge et al., 2001) as a proxy for urban NO_2 emissions. Monthly-mean ERS-2 Along-Track Scanning Radiometer (ATSR) fire counts (Arino and Melinotte, 1999) serve as a proxy to exclude areas recently exposed to biomass burning. These maps capture the seasonal variability of biomass burning patterns.

Application of the criteria to accept or reject grid cells based on OLS and ATSR data is tabulated in Tables 2 and 3. Masking based on OLS data effectively excludes large areas in South America, South Africa, Perth and vicinity, and Eastern Australia.

In spite of the masking described above, it cannot be ruled out that NO_x produced in urban or biomass burning may still affect the comparison. Boundary-layer NO_2 has a lifetime of 6–24 h (Beirle et al., 2003), long enough to occasionally cross distances of the order of 100–500 km and flow into our analysis area. This is the main motivation to mask also adjacent grid cells in situations of high fire counts and high relative light intensity. NO_2 that is rapidly transported upward and out of the boundary-layer, for instance by the same deep convective processes that are associated with lightning NO_x production, may live even longer. This potential error source will be discussed in more detail in Sect. 4.3.2.

4.3. Correlation between GOME NO_2 and modelled LNO2

As an example we present the 1997 annual mean correlation (1997) between GOME observed tropospheric NO_2 and collocated TM3 LNOx for Australia in Fig. 6. Only

ACPD
5, 3047–3104, 2005

observations with a cloud reflectance fraction less than 50% have been selected, corresponding to FRESCO cloud fractions smaller than ≈0.15. Modelled and observed columns are stored on the 2.5°×2.5° TM3 grid. Only grid cells with at least three GOME observations were used in the analysis. The good correlation coefficient (r=0.82) demonstrates that, on average, observed patterns of NO_2 are in good agreement with simulated LNO2 patterns over Australia. For all regions we find convincing annual correlations with coefficients ranging from 0.66 to 0.91 (not shown). For CP-simulated LNO2 we find similar high spatial correlation coefficients (not shown).

4.3.1. Spatial and temporal correlation methods

In the comparisons between modelled and observed NO_2 fields we focus on the spatial and temporal patterns, and not on the average NO_2 amounts (background). Modelled and observed lightning NO_2 columns are generally <0.5 10^{15} molec.cm^{-2}, and even a small bias in observed NO_2 may lead to considerable errors in an estimate of the ratio between observed and modelled NO_2. This statistical pattern-amplitude comparison method is less sensitive to possible offsets in either modelled or observed columns.

Correlations in space and time between GOME and model are studied independently. The temporal approach compares the time dependence of modelled LNO2 and observed NO_2 at a given location and consists of a linear least squares regression of modelled LNO2 and observed total NO_2 for a particular grid cell i. Taking into account all data for 1997 results in slope s_i and intercept o_i for every individual grid cell. The regressions also account for errors on the individual observations. A minimum of at least 5 observations in 1997 is required for a grid cell to be included in the comparison. Subsequently, the 1997 average regional slope is determined as a weighted mean of the individual grid cell slopes:

$$\bar{s}_t = \frac{\sum_{i=1}^{n} s_i w_i}{\sum_{i=1}^{n} w_i}, \quad (3)$$

with w_i the inverse of the variance of s_i.

The comparison in temporal variability between TM3 LNO2 and GOME NO_2 columns is illustrated for a grid cell in the Congo basin. The left panel of Fig. 7 shows a time-series of TM3 LNO2 (triangles) and GOME (squares) NO_2 columns at 8.75° S, 18.75° E for observations with cloud reflectance <50%. The period covers January-April 1997 before the start of the biomass burning season in the grid cell. The right panel shows the corresponding correlation and least squares fit of the timeseries with a correlation coefficient of 0.78 and a slope of 2.38 (n=14).

In the spatial correlation method, data of one day is compared for a complete region, with the regions defined in Fig. 10. A plot of all pairs of model LNO2 and GOME NO_2 values results in a slope s_d and intercept o_d for a given day. At least 5 gridcells with observations are required for a day to be included in the analysis. Subsequently a weighted mean for 1997 is computed based on the individual values for s_d:

$$\bar{s}_s = \frac{\sum_{d=1}^{n} s_d w_d}{\sum_{d=1}^{n} w_d}, \quad (4)$$

with w_d the inverse of the variance of s_d, and n the number of days for which a slope was computed.

Spatial patterns related to LNO2 emissions may well resemble NO_2 patterns related to other emissions such as biomass burning. For instance, slopes in NO_2 between land and sea are common to most sources of NO_2 as their origins are concentrated over continents. The temporal correlations, in contrast, are not influenced by such an overlap of emission areas. We expect that temporal patterns for individual sources are more different because lightning, biomass burning and soil NO_x emissions all have their own characteristic temporal behaviour. As a consequence, the spatial and temporal correlation approaches can be seen as largely independent methods to estimate the LNO2 concentration.

ACPD
5, 3047–3104, 2005

4.3.2. Correction for other sources

The intercept of regressions like the one shown in Fig. 6 can be interpreted as that part of the NO_2 observation which has a pattern orthogonal to the modelled LNO2. This background part is attributed mainly to sources other than lightning. The intercept in Fig. 6 ($+0.24\times10^{15}$ molec.cm^{-2}) is small compared to the range of values found. Similar small intercept values between -0.05 and 0.20×10^{15} molec.cm^{-2} are found for other regions. These results show that our masking scheme is efficient in reducing the influence of other sources, enhancing the significance of the regressions.

However, part of the NO_2 distribution resulting from other emissions will not be orthogonal to the LNO2 distributions. The slopes s of the regressions as shown in Figs. 6 and 7 need to be corrected for contributions from other sources that have similar patterns as LNO2. This is done by simulating GOME observations with TM3 for the same subset of observations, and computing slopes s_{sim} between these simulated observations of the total NO_2 column and the simulated LNO2. In other words, we compute again slopes following Eqs. (3) and (4) but now by comparing TM3 total NO_2 to TM3 lightning NO_2. Hence, the slope s_{sim} is representative for the modelled ratio of $<x_L + x_O, x_L>/<x_L, x_L>$ where $<>$ denotes the covariance. This can be written as $1.0 + x_O/x_L$ for the part of x_O that correlates positively with patterns of x_L, with x_L the simulated LNO2 column and x_O the simulated contributions of other sources to the total NO_2 column. The other sources include soil and biomass burning emissions, as well as inflow of industrial emissions. Subsequently, we account for the influence of other sources by subtracting the slope correction term ($s_{sim}-1$) from s.

Slope corrections ($s_{sim}-1$) range from +0.08 to +0.46 for the CP parametrisation and from +0.15 to +0.43 for the H5 scheme. For cloudy situations we find similar slope corrections. Table 4 summarizes the results of the simulation for both the temporal and spatial methods for both schemes for clear-sky scene situations. Indeed, results from the spatial correlation method are influenced by other sources of NO_x with similar spatial patterns. This is reflected in, on average, slope correction terms that exceed

ACPD
5, 3047–3104, 2005

the slope correction terms for the temporal method by +0.07. Intercepts are (0.02–0.11)×10^{15} molec.cm^{-2}, giving an estimate of NO_2 from other sources in TM3 with patterns orthogonal to LNO2. Generally, slope corrections are smaller than the slopes from the GOME-TM3 comparison themselves, providing confidence in the final results.

One source of NO_x that interferes with LNOx are soil emissions. In TM3 a time-independent climatology of soil emissions is used, that does not take into account that soil emissions are triggered by precipitation ("pulsing", Yienger and Levy, 1995). The annual pulsing soil NO_x emission budget is estimated to amount to 1.3 TgNyr^{-1} (Yienger and Levy, 1995), compared to approximately 5 TgNyr^{-1} from lightning. Because pulses last for several days, only a fraction of the pulsed NO_x will be transported to high altitudes by uplifting in convective systems, and NO_x concentration patterns from soil pulsing will not fully coincide with LNOx patterns. Moreover, Huntrieser et al. (1998) found that over Europe, with high levels of boundary layer NO_x, still more than 80% of the NO_x in large thunderstorms originated from lightning. We estimate that boundary layer NO_2 columns for summertime Europe are at least 50 times larger than daily columns from soil (0.1×10^{15} molec.cm^{-2}, Beirle et al., 2004; Jaeglé et al., 2004), so we expect the systematic effect of "pulsing" on UT NO_x levels to be small.

The uncertainty estimate for the slope correction (s_{sim}−1) is based on the combined estimates of soil and biomass burning emission uncertainties. Soil emissions in TM3 are 5.5 Tg N/yr after canopy reduction (Yienger and Levy, 1995) with an uncertainty of 40%. TM3 biomass burning emissions are 6.9 TgN in 1997, and as a measure of the uncertainty we use a number obtained from Duncan et al. (2003) who report an interannual variability in biomass burning emissions of approximately 10%. Error estimates for the slope corrections have been obtained by applying a 10% increase and decrease in biomass burning and 40% increase and decrease in soil emissions. From these runs, we arrive at uncertainties in s_{sim}−1 of 0.02–0.15.

4.4. Mean regional slopes

Results of statistical regressions can be misleading and are easily overinterpreted. This is a main motivation to investigate as many inependent estimates as possible. The spread in values found then provides an independent error estimate and is a check for the robustness of conclusions drawn. Independent analyses have been performed for:

- The subset of cloud-free and cloudy observations.
- The temporal and spatial correlation methods.
- The CP and H5 parametrisation schemes
- The various tropical regions.

Regional mean slopes and intercepts corrected for the influence of non-lightning NO_x sources are presented in Fig. 8. The upper panel of the Figure shows the results for the CP scheme, and the lower panel for the H5 scheme for both the spatial and temporal method in situations of clear-sky GOME observations. Over the tropical continents mean slopes for the CP scheme are 0.9 for Africa and 1.4 for Australia, clearly higher than over South America (0.6). For the H5 scheme mean slopes over tropical continents are all close to 1.0 for both the spatial and temporal method, indicating a remarkable agreement in modelled LNO2 and observed NO_2. Over tropical oceans both the H5 and CP scheme significantly overestimate LNO2 concentrations. The error bars on the slopes have been computed as the combined uncertainty on $s_{s,t}$ and s_{sim}. Here we express the error variance of the mean regional slopes by adding contributions from the estimated error in the regression coefficient and from the estimated error in the slope correction term, i.e. $\langle \epsilon^2 \rangle = \sigma^2_{s_{s,t}} + \sigma^2_{sim}$.

There is a number of model lightning parametrisation aspects that may explain the regional differences in slopes:

- CP (specific). The CP scheme assumes a constant rainfall to lightning flash ratio. However, there are several papers reporting on strong regional differences in

rainfall-to-lightning flash ratios between different continents (e.g. McCollum et al., 2000), and between continents and oceans (e.g. Allen and Pickering, 2002).

– Both schemes assume that the energy ratio of CG and IC flashes equals 10. However, Gallardo and Cooray (1996) found that this ratio is more likely to have a value of approximately 1.0. As the (occurence) fraction of IC lightning flashes of total lightning is higher over continents than over oceans (e.g. Kurz and Grewe, 2002), a CG:IC energy ratio of approximately 1.0 would effectively reduce the overestimation in LNO2 produced over oceans.

– Both schemes also assume that convective intensity is 10 times stronger over continents than over ocean. Strong overestimations in parametrised marine lightning flash ratios have been found for the H5-scheme by Jourdain and Hauglustaine (2001) who assumed a similar (5 times) convective intensity ratio. Increasing the continent divided by ocean convective intensity ratio would effectively reduce the overestimation in LNO2 produced over oceans, due to the scaling to a fixed global annual LNOx production.

With respect to this last issue, it is interesting to note that the observed continent divided by ocean LNO2 production ratio presented in Sect. 3 has a value of only 1.6 at 10:30 h local time, apparently in contrast with a value exceeding 10 required here. However, convective activity over land is at a distinct minimum at 10:30 h local time, and the continent:ocean ratio is expected to be much higher in the afternoon. For instance, TRMM data (Ushio et al., 2001) could be used to investigate the diurnal cycle of continent divided by ocean lightning activity.

As discussed in Sect. 3, cloudy observations are sensitive to errors in the vertical distribution of NO_2. Nevertheless, they constitute an independent data sample and we may interpret the results from the cloudy analysis as independent from the clear-sky results. The NO_x originating from lightning will largely reside above the cloud cover, where GOME has a large sensitivity compared to clear-sky. Boundary layer pollution, on the other hand, will be effectively shielded from view by the presence of clouds and

near-ground contributions to the NO_2 column will influence the comparison differently. The study for cloudy grid cells shows similar results for most regions except for South America and the Indian Ocean (Fig. 9).

For the CP scheme, considerable differences are found over South America. Cloudy-sky situations give a slope that is 0.4 smaller than for clear sky. Over the Indian Ocean the spatial correlation method gives a slope that is 0.5 larger for cloudy than for clear-sky situations, opposed to an insignificant difference for the temporal method. For the H5 scheme, cloudy-sky slopes are 0.6 smaller than clear-sky slopes. Over the Indian Ocean the spatial method gives a slope that is 0.5 higher thanthe slope from the temporal method, just as in the CP analysis.

The higher slopes for clear observations over South America may be related to the fact that cloud-covered observations have mainly been taken in the rainy season and cloud-free observations mainly during the rest of the year. For all regions apart from South America, the average difference between clear and cloud covered observed columns is $+0.01\times10^{15}$ molec.cm^{-2}. South America, however, shows clear-sky columns that are on average $+0.15\times10^{15}$ molec.cm^{-2} larger than cloudy-sky observations. As correlation coefficients for the clear (r=0.77) and cloudy-sky (r=0.69) situations are similar, this may indicate that the cloud covered data sample over South America is likely to represent a different lightning regime. Cloud cover is highest over South America in the DJF and SON seasons, and these seasons appear to have less LNOx production than modelled in the MAM and JJA seasons.

The difference between cloud covered results for the temporal and spatial methods over the Indian Ocean may well reflect the enhanced sensitivity of the spatial method for similar spatial patterns from other NO_x sources. Plumes of tropospheric NO_2 originating from Africa and Indonesia can develop during the monsoon transition periods over the Indian Ocean as described by Kunhikrishnan et al. (2004). These plumes are associated with enhanced mid-tropospheric NO_2 concentrations originating from mainly biomass burning in Africa and Indonesia. Especially in so-called monsoon transition periods such as April-May, and September-October, NO_x from continental sur-

face sources is transported to the MT and UT by deep convection. The continental MT and UT NO_x subsequently follow the same transport pathways as UT LNOx, resulting in a similar spatial distribution of biomass burning NO_x and LNOx over the Indian Ocean. These similar patterns may well explain the enhanced spatial slope relative to the temporal slope. The temporal method is designed to track variations with time at one given location and hence additional NO_x increases from other sources are more likely to result in higher intercepts than in higher slope values. Indeed, the temporal scheme features intercepts over the Indian Ocean higher by +0.30 (CP), +0.43 (H5) compared to the spatial method. The fact that there is no significant difference between the two methods for clear-sky situations may therefore be related to the fact that the cloud-free observations do not sample the monsoon (i.e. clouded) transition period.

5. Tropical LNO2 maps

Figure 10 shows the modelled LNO2 for the CP and H5 schemes and the GOME observations for 1997, corrected for estimated contributions of other sources of NO_x. This contribution is taken as $x_O = (g_{sim} - 1.0) \cdot x_L + o$ with $s_{sim} - 1.0$ the slope correction from Table 4, x_L the modelled LNO2 column, and o the intercept. It is important to note that the maps of Fig. 10 represent the annual mean LNO2 distribution. Note that slopes as discussed above can not be directly inferred from these plots, since these are determined from modulations (in space and time) on top of the average patterns in Fig. 10. The purpose of these maps is mainly to visually compare average modelled and "observed" LNO2 patterns.

The TM3 simulations and measurements are shown for clear-sky situations only in 1997. Over the large ocean regions where no masking is applied and many clear-sky observations are available, the fields represent a yearly average. Over continents, the fields should not be regarded as annual means, as grid cells may have been sampled during one season or for a few occasions only due to masking or few available cloud-free observations.

ACPD
5, 3047–3104, 2005

Both TM3 and GOME NO_2 in Fig. 10 show enhanced values over the tropical continents. Also the 'outflow' patterns off the South American West coast and – in the CP scheme – for the Eastern Atlantic seem to agree reasonably. But there are also distinct differences: TM3 shows higher lightning NO_2 values than GOME over most of the oceans, consistent with the low slope values in Fig. 8. Furthermore it shows that the GOME fields exhibit much stronger spatial variability than TM3. This may be related to observational noise and the incomplete removal of contributions of other NO_2 sources affecting the comparison.

6. Global LNOx production in 1997

In the previous section we have shown that observed GOME NO_2 values correlate well with model predicted patterns of NO_x produced by lightning. The Southern Hemisphere tropical regions used in our study contain a considerable fraction of the total global LNOx source, namely about 35–50%. Therefore we can use the GOME/model slopes to derive a top-down estimate of the global LNOx production.

6.1. Approach

The ratio between observed and modelled atmospheric quantities of LNO2, is given by regional slopes s_j with j the index number for a region (j=1 for the Pacific Ocean, j=2 for South America and so on). Hence, the annual LNOx production P_G is estimated by rescaling the modelled production P_T as follows:

$$P_G = P_T \frac{\sum_j s_i \bar{x}_j a_j}{\sum_{j=1}^{n} \bar{x}_j a_j}, \quad (5)$$

with x_j the mean simulated LNO2 column, and a_j the total surface of area j.

ACPD
5, 3047–3104, 2005

6.2. LNOx production in the 40° S–5° N area

Application of Eq. (5) with j=1,...,6 allows for a direct rescaling of the modelled production P_T over the 40° S–5° N area. The slopes s_1 to s_6 are directly deduced from Figs. 8 and 9. We assume that the annual average net transport of LNO2 into the 40° S–5° N area is negligible. Note that LNOx transport between the regions 1 to 6 is considerable, making it difficult to estimate the production per region. Furthermore we also assume that chemistry can be approximated to be linear in the TM3 difference run.

For the CP scheme, 2.7 TgN is produced in the 40° S–5° N area. This production is rescaled directly with the slopes presented in Fig. 8. Using slopes from the temporal correlation method for clear-sky observations, this approach rescales the modelled 2.7 TgN LNOx production to 1.1 TgN. For the H5 scheme, 2.2 TgN is produced in the 40° S–5° N area and this is rescaled with the slopes obtained with the temporal correlation method for clear-sky situations to 1.0 TgN. This number is very close to the rescaled value of 1.1 TgN obtained for the CP-scheme, even though the original CP and H5 LNOx production differed by (2.7–2.2=) 0.5 TgN.

6.3. Global LNOx production

An estimate of the annual global LNOx production P_G requires important assumptions on the observation/model slopes outside the 40° S–5° N area. We arrive at an estimate from Eq. (5) for j=1,...,10, where s_7 (continent) and s_8 (ocean) are the estimated slopes for the 5° N–30° N area, and s_9 (continent) and s_{10} (ocean) the same for the rest of the world. The basic assumption is that we may use the mean continental and ocean slopes derived from the 40° S–5° N area for $s_7 - g_{10}$.

In the CP scheme, more than 50% of the LNOx production takes place outside 40° S–5° N, and these emissions can only be rescaled indirectly. For these areas we assume for oceans s_7, s_9=0.93 and for continents s_8, s_{10}=0.21, corresponding to the mean continent and ocean slopes determined in the 40° S–5° N regions for the CP scheme. The values for x_j and s_j outside the tropical areas have been derived from the same

ACPD
5, 3047–3104, 2005

model runs as used to determine the slopes within the analysis area. Using s_7 and s_8 in 5° N–30° N, we find that the LNOx production there is rescaled from 2.5 to 1.7 TgN in 1997. Outside of the tropics, LNOx production is rescaled through s_9, s_{10} from 0.5 to 0.4, a relatively small reduction as the relative area of continents is larger than in the Southern Hemisphere. In effect, the global LNOx production is rescaled from 5.7 to 3.2 TgN.

In the H5 scheme, more than 60% of the LNOx production takes place outside 40° S–5° N. Using s_7, s_9=0.19 and s_8, s_{10}=1.03, we find a LNOx reduction outside 40° S–5° N from 4.2 TgN to 3.6 TgN. Thus, the global LNOx budget for 1997 for the H5 scheme is rescaled from a model value of 6.4 to (1.0+3.6=) 4.6 TgN. The difference with the 3.2 TgN derived for the CP-scheme is largely due to extrapolation assumptions, as the rescaled values within the 40° S–5° N area are only 0.1 TgN apart.

In this work 8 methods, of which 4 are independent, to determine slopes s_j have been applied. Table 5 summarizes the estimates for the global LNOx production based on the results from the 8 experiments. The arithmetic mean of the 8 experiments is 3.5 TgN, and individual results range from 2.3–4.6 TgN. The H5 results are on average systematically higher by about 1.5 TgN than the CP results. This is mainly a consequence of the determination of the budget outside the 40° S–5° N analysis area as all methods give very similar results within the analysis area.

6.3.1. Random errors

The errors in s_j are estimated from combining the errors associated with the statistical comparison and the errors in the slope correction term. The uncertainty in s_j is thus determined by GOME observation errors, model pattern errors (i.e. meteorology) and by errors in the modelled strength of other NO_x sources.

Random errors in P_G have been determined from errors in the individual slopes s_j. As explained above, the slopes of the individual regressions contain uncertainties that account for both the spread of points around the straight line fit, and GOME retrieval errors. Subsequently the uncertainty-weighted mean of these individual regressions for

region j is determined (e.g. averaging over grid cells for the temporal method). In the 40° S–5° N area, these correspond to the uncertainties reported in Figs. 8 and 9. These slope errors are typically between 0.1 and 0.2. In the 5° N–30° N area, we assume that the standard deviation from the mean (ocean, continent) derived for regions 1 to 6 is a reasonable estimate for the uncertainty in s_7 and s_8 since this area is still characterised as 'tropical'. These uncertainties are on average 0.3. For the extratropical slopes s_9 and s_{10}, we conservatively estimate the uncertainty to be 1.0. A measure of the random error in the overall global production P_G can be determined with two methods:

– The random error (or standard deviation) in a single estimate of the global LNOx production can be obtained if we assume that errors in the slopes are uncorrelated. The error variance $\langle \epsilon^2_{P_G} \rangle$ is calculated from the error propagation of uncertainties in the regional slopes s_j as:

$$\sigma^2_{P_G} = \langle \epsilon^2_{P_G} \rangle = \sum_{j=1}^{10} \left(\frac{P_T \cdot \bar{x_j} \cdot n_j}{\sum_{j=1}^{10} \bar{x_j} \cdot n_j} \right)^2 \sigma^2_{s_j}. \quad (6)$$

The uncertainties σ_{P_G} for the 8 estimates are in the 0.7–1.5,TgN range with an average value of 1.0 TgN. Table 5 quotes the individual uncertainty estimates in P_G. The random error for the estimate of the LNOx production within the 40° S–5° N area is on the order of 10%–20% only.

– We can use the spread in values of the 8 experiments as estimate of the error on the mean. The data set presented in Table 5 has a standard deviation of 0.9 TgN.

These two independent ways of estimating the random error produce a very similar result. The value for the statistical error seems to indicate that we have obtained a rather precise estimate of the LNOx production. Taking the arithmetic mean we arrive at 3.5±0.9 TgN.

6.3.2. Systematic errors

One approach in estimating the systematic error in P_G (B_{P_G}) is to assume that the errors in the slopes s_j are correlated. In such an approach, errors in the GOME observations and in the GOME-model comparison are interpreted as biases. A first order estimate of the deviation from the true value for P_G may then be obtained as follows:

$$B_{P_G} = \sum_{j=1}^{10} \left(\frac{P_T \bar{x_j} n_j}{\sum_{j=1}^{10} \bar{x_j} n_j} \right) \sigma_{s_j}. \quad (7)$$

For B_{P_G} we find values between 1.0 TgN (CP, clear sky, spatial method) and 2.3 TgN (H5, cloudy sky, temporal method) with an average of B_{P_G}=1.4 TgN.

Apart from this approach, there may be important systematic errors related to (1) the GOME observations, to (2) the model, and to (3) the regressions. Each of these types of errors in discussed below.

6.3.3. GOME errors

Not all systematic errors in GOME observations introduce errors in the slopes in Table 5. If the observed columns suffer from a constant bias, this will result in an increase (decrease) of the offset o_j, and not translate in a systematically erroneous s_j value. Only if a bias scales with the reported column value, s_j will be in error. Thus, as GOME columns are inversely proportional to the air mass factor, systematic overestimations in the AMF are expected to lead to underestimated slopes. However, most of the LNO2 is deposited in the upper troposphere where GOME has a high sensitivity and AMF errors are generally small. Systematic AMF errors are to be identified and eliminated, which is beyond the scope of this paper.

There may also be difficulties in accurately observing patterns of NO_2 because there may be stratospheric patterns which are not modelled well in the assimilation part of the retrieval approach. However, since the results in Table 5 for cloud-free and cloud-

covered scenes are consistent, this strengthens our confidence in the GOME retrievals and both AMF and assimilation errors are likely small.

6.3.4. TM3 errors

In our method to rescale modelled regional LNOx productions, we need to be especially suspicious of the model's capability to accurately reproduce spatial and temporal patterns of LNO2. Systematic model errors are not easy to quantify, and we have chosen a practical approach to assess the possible impact on our production estimates. The following gives an overview of possible systematic model errors:

- Incorrect NO_x lifetime.
- Errors in the vertical distribution of LNOx production.
- Errors in photo-chemistry.
- Errors in parametrisation of convection and cloud top heights.

A reasonably well described lifetime in TM3 is essential to estimate the production of LNOx from modelled and observed concentrations of NO_2. An incorrect NO_x lifetime would result in too high or low overall concentrations if transport is descibed realistically. This would in turn lead to systematic errors in the slopes. The literature however provides support that TM3 produces realistic NO_x distributions. For instance, we note that various studies (Emmonds et al., 1997; Wauben et al., 1997; Meijer et al., 2000) have indicated that TM3 is capable of reproducing aircraft- and surface-observed NO_x concentrations for a range of different meteorological and chemical situations. Also, recent studies by Brunner et al. (2003, 2005) showed that TM3 is well capable of reproducing observed NO_x and NO_x-related species.

The vertical distribution of LNOx influences the horizontal distribution and observed spatial patterns. We expect that the effect of errors in the vertical distribution of LNOx is small. For instance, both Kurz and Grewe (2002) and Jourdain and Hauglustaine

(2001), using similar parametrisations to the CP and H5 schemes respectively, found large flash density overestimations over oceans. Therefore we argue that the overestimations of oceanic LNO2 that we find are a result of flash density overstimation rather than the result of errors in the modelled vertical distribution of lightning NO_x. Moreover, a recently submitted paper by Labrador et al. (2004b) shows little difference in LNOx concentrations for model runs with the vertical LNOx distribution according to Pickering et al. (1998) and a vertical distribution in the 5 highest layers of the convective cloud. The same is found by Olivié et al. (2005)[2] who used a lightning parametrisation based on convective updrafts.

The relation between LNOx production and the NO_2 concentration in the atmosphere is in reality non-linear. The scaling of the LNOx budget based on the slopes observed neglects this non-linearity. This may be an issue especially for the oceans where the slopes found are significantly smaller than one. The partitioning of nitrogen between NO_2 and NO, and between NO_x and NO_y is also a potential source of model error. Even if the lifetime of NO_x and NO_y is modelled correctly, errors in the NO_2:NO ratio, for instance due to errors in the modelled ozone concentration, would result in incorrect slopes. Fortunately, Brunner et al. (2005) show that a comparison of TM3 modelled ozone and in situ measurements of ozone over the South Pacific gives quite reasonable agreement, indicating that slope errors due to ozone errors over the South Pacific are likely small.

The description of clouds in numerical weather prediction analyses is known to be problematic, especially in the tropical regions. The modelled LNOx is sensitive to a correct timing and strength of convective complexes. The representation of these processes on the model grid of 2.5 degree resolution causes additional errors. Nevertheless, we found on average good correlations between modelled LNO2 and observed NO_2 columns, indicating that the major features of NO_2 distribution resulting from modelled convection-related emissions and subsequent transport are realistic.

[2]Olivié, D. J. L., Meijer, E. W., and van Velthoven, P. F. J.: Parameterisation of the production of NO_x by lightning for global chemistry transport models, in preparation, 2005.

6.3.5. Comparison errors

Apart from errors directly related to the TM model and to GOME, there are also errors that may result from our statistical analysis, indirectly related to GOME and model errors. Therefore, we set up a simple study to provide a qualitative estimate of errors that may occur in the comparison of patterns in independent data sets. The upper panels of Figs. 11 and 12 show fictitious modelled (solid line) and observed (dashed line) patterns. The observations are based on assumed 'true' patterns (shown as dotted line) with added random observational noise. Subsequently, the pattern was simulated with a model that suffers from two types of systematic errors. These errors are either a (spatial or temporal) mismatch with the 'true' pattern (a shift, Fig. 11), or an exaggerated (spatial or temporal) smearing or diffusion of the 'true' pattern (Fig. 12).

The spatial correlation method is sensitive to errors in the spatial distribution of LNO2 patterns. Relevant systematic errors are to be expected in the modelling of the transport, lifetime and vertical distribution of LNO2. The shift experiment also has an interpretation for the temporal method, as LNOx production may take place too early or too late in the parametrisations, leading to a shifted temporal pattern

Processes such as deep convection typically take place on a scale much smaller than the size of a grid cell. For instance, in the H5 scheme ECMWF cloud heights are sampled once every 6 h, giving instantaneous values, clearly too low to properly resolve much shorter periods of thunderstorm and lightning activity. The model may thus suffer from errors in representing such processes. Furthermore, numerical diffusion in the advection, vertical transport processes and the limited resolution of the model tend to smoothen NO_2 structures. Part of this effect is taken care of by averaging the GOME observations over model grid cells before making the comparisons. To simulate this effect we also study the correlation of the "true" toy pattern with a smoothed (smeared) version.

The lower panels of Figs. 11 and 12 show the result of our systematic error study. One important requirement in this study is that the correlation coefficients between

ACPD
5, 3047–3104, 2005

'observed' and 'modelled' patterns do not fall below ~0.65, the lowest regional value found in our 1997 average correlation of GOME and TM3 columns.

The upper plot of Fig. 11 shows a model pattern shifted by −50% relative to the width (0.3 x-axis units) of the 'true' pattern. The observed pattern follows the 'true' pattern but has an additional random error that is typical for gridded GOME observations. The lower panel shows the regression plot corresponding to the data presented in the upper panel: the solid line gives the least squares regression fit (s=0.88±0.26), and the dashed line gives the $y = x$ line (s=1.00) that we expect if the model and observations would agree. The correlation coefficient r=0.66 for this example. By repeating this experiment with random noise a 1000 times we arrive at, on average, a systematic slope underestimation Δg=−0.20(±0.13) and Δo=+0.05 for a mean correlation coefficient r=0.70. Apparently, a (spatial or temporal) shift of half a unit (i.e. half a grid cell, half a time step) results in underestimations of the slope of approximately 20%.

We conducted a similar experiment with a model pattern smeared by 50% (width now 0.45 x-axis units) relative to the 'true' width of the pattern. No shift was assumed and the random errors are similar to the previous experiment. The lower panel of Fig. 12 shows a regression fit with a s=1.44 (±0.37) for an r=0.65. Repeating this experiment 1000 times we arrive at a significant systematic slope error of Δg=+0.35(±0.18) and Δo=−0.10 for a mean correlation coefficient r=0.83. In conclusion, if the model smears 'true' patterns systematically by 50%, slopes may be overestimated by up to 35%. Note that a smearing factor of 50% is on the high side and that possible systematic 'smearing' errors such as diffusion, or representativity of instantaneous cloud heights, are likely less than 50%.

Generally, a strong shift in a modelled pattern results in a loss of correlation between model and observation. In such situations, a model-observation scatter shows a strong scatter of points. A strong smear effect in TM3 is expected to result in a strong, non-linear shape of the distribution of points in a model-observation comparison. Since neither of these are observed in Fig. 6 nor in any of the annual average correlation figures for the other continents (not shown), it seems that neither shift nor smearing

ACPD
5, 3047–3104, 2005

errors in TM3 have systematically influenced the results in Table 5. This also follows from our simple experiment: shifts and smears up to 60% are still consistent with correlations found in the GOME-model comparison (minimum r=0.65). The errors from the shift and smearing experiments are (−20%,+35%) and from these numbers we conservatively estimate the systematic error to amount to an additional error of (±)35% in the estimated global LNOx production budget. As the signs of these effects are opposite, we expect at least a partial cancellation of errors from shift and smear effects.

6.3.6. Total error estimate

Model shifts and smears are just two examples of possible systematic errors. Nevertheless, their effects may lead to systematic errors with opposite signs. CTM-experiments typically suffer from a variety of possible systematic errors, and therefore an ensemble of systematic errors is sometimes treated as a random error. Subsequently we proceed by combining all the errors as though they were random and independent:

$$\sigma^2_{final} = \langle \epsilon^2_{random} \rangle + \langle \epsilon^2_{syst} \rangle. \quad (8)$$

We calculate total errors for the 8 individual estimates of the LNOx production budget given in Table 5 by using Eq. (8). The systematic error $\langle \epsilon_{syst} \rangle$ is assumed to be 0.35. Results are summarised in Table 5 in the column headed 'Total error'.

In summary, the results of the 8 experiments range from 2.3–4.6 TgN, largely due to systematic errors associated with extrapolation of the slopes to areas of the globe not covered by our analysis. A more conservative view consists of taking the largest and smallest P_G values from the 8 readings and adding resp. subtracting the estimated standard error in P_G. This leads to an estimated LNOx production in the 1.1–6.4 TgN range.

7. Conclusions and outlook

Nitrogen dioxide measurements of GOME are sensitive to NO_2 produced by lightning. In situations with high clouds, the tropospheric NO_2 column shows a rapid increase consistent with the parametrisation of Price and Rind (1992). The observed increase can be well described with an empirical power-law, where the LNOx increases with the cloud top height as $H^{4.9\pm2}$. The uncertainty in the observed value of the power is estimated to be 40% related to assumptions with respect to background NO_2 concentrations. We interpret this relationship as strong evidence that GOME is capable of detecting LNOx production. From the ratio of the increases found over continents and oceans, we estimate that continental updrafts are stronger by a factor of 1.6 in producing LNOx at the 10:30 h local time of observation.

Modelled LNO2 and observed tropospheric NO_2 patterns are found to correlate surprisingly well, with spatial correlation coefficients $r \approx 0.80$ in 1997 in six distinct tropical regions between 40° S and 5° N. We use spatial and temporal correlations to determine linear regression coefficients for these 6 tropical regions. The intercept of these regressions show that these regions are little affected by NO_x emissions from other sources. The slopes, corrected for possible influences of other NO_x sources, indicate that TM3 significantly overestimates LNOx emissions over the oceans. Over tropical continents, we find a good quantitative agreement between modelled LNO2 and observed NO_2. This is true for two different lightning parametrisations, one based on convective precipitation, and one based on the fifth power of the cloud top height. The modelled overestimations over oceans may be reduced if the assumed energy ratio (10:1) between cloud-to-ground and intra-cloud lightning is decreased. An increase in the assumed ratio (10:1) between continent-to-ocean convective intensity is also expected to reduce modelled oceanic LNOx overestimations. This work also suggests that for the convective precipitation scheme, there are significant regional differences in rainfall-to-lightning ratios that should be accounted for.

By rescaling the original LNOx production modelled by TM3 for the year 1997, 8

estimates of the global LNOx production have been obtained. We find that the LNOx production between 40° S and 5° N amounts consistently to ∼1.0±0.2 TgN for both the CP and H5 schemes. Here the error bar accounts for random errors only. Assuming that the slopes may be extrapolated to the rest of the world, we arrive at a global LNOx production of approximately 2.8 TgNyr^{-1} for the CP and 4.3 TgN for the H5 model version. The difference between these two estimates is largely due to assumptions with respect to extrapolating slopes to the rest of the world. Random errors in these estimates are dominated by errors in the observations and in the correction of the slopes for the influence of other sources. Accounting for random errors the LNOx production is estimates as 3.5±0.9 TgN in 1997. Accounting for random and systematic errors, as well as the range of independent estimates, LNOx production is conservatively estimated in the 1.1–6.4 TgN range.

This study presents a first attempt to estimate the global LNOx production by comparing observed NO_2 with modelled LNO2 distributions. Such estimates can be extended by repeating this method for all years between 1996 and 2004, covered by the GOME and SCIAMACHY measurements, as well as future NO_2 observations provided by OMI and GOME-2 can be included. Especially NO_2 and cloud observations from OMI are expected to contribute to improved estimates of LNOx: the small OMI pixels of 13×24 km^2 are better suited to resolve convective complexes. Also, the OMI 13:30 h local time overpass time is closer to the maximum in the diurnal cycle of convective activity over continents.

Future work should investigate the effect of reduced CG:IC energy ratio's and increased convective intensity ratio's on the capability of models to reproduce observed LNO2 patterns. Recently, TM3 has been extended with an updraft velocity-based lightning scheme that has shown promising results in the literature (Allen and Pickering, 2002; Kurz and Grewe, 2002, Olivié et al., 2005[2]). LNO2 patterns modelled with this scheme are to be compared to satellite data. Moreover, a proper description of convective activity in chemistry-transport models remains crucial for accurate parameterisations of lightning activity. Convective mass fluxes are not always stored in operational

meteorological data and in such situations simplified schemes are used for diagnosis. More advanced schemes for the diagnosis of convective mass fluxes in chemistry transport models are clearly needed. Also, the temporal and spatial scale of lightning activity is much smaller than most model resolutions. Hence, increasing the model resolution is expected to improve the description of convection and convection-related processes such as lightning.

Acknowledgements. The authors acknowledge S. Beirle and T. Wagner (IUP-Heidelberg) for providing the GOME DOAS NO_2 slant columns and for stimulating discussions. M. van Weele and P. van Velthoven are acknowledged for advice on the TM3 model and comments. This work was supported by the EU GOA (contract EVK2-CT-2000-00062) and ASSET (contract EVK2-CT-2002-00137) projects.

References

Allen, D. J. and Pickering, K. E.: Evaluation of lightning flash rate parameterizations for use in a global chemical transport model, J. Geophys. Res., 107, 4711, doi:10.1029/2002JD002066, 2002. 3067, 3081, 3088

Arino, O. and Melinotte, J. M.: The 1993 Africa fire map, Int. J. Remote Sens. Environ., 69, 253–263, 1999. 3061

Beirle, S., Platt, U., Wenig, M., and Wagner, T.: Weekly cycle of NO_2 by GOME measurements: A signature of anthropogenic sources, Atmos. Chem. Phys., 3, 2225–2232, 2003, SRef-ID: 1680-7324/acp/2003-3-2225. 3061

Beirle, S., Platt, U., Wenig, M., and Wagner, T.: NO_x production by lightning estimated with GOME, Adv. Space Res., 34, 793–797, 2004. 3049, 3050, 3065, 3088

Boersma, K. F., Eskes, H. J., and Brinksma, E. J.: Error analysis for tropospheric NO_2 retrieval from space, J. Geophys. Res., 109, doi:10.1029/2003JD003962, 2004. 3049, 3052, 3053, 3060

Brunner, D. W. and van Velthoven, P.: Evaluation of Parameterizations of the Lightning Production of Nitrogen Oxides in a Global CTM against Measurements, Eos, Transactions, 80, 46, F174, 1999. 3058

Brunner, D., Staehelin, J., Rogers, H. L., et al.: An evaluation of the performance of chemistry transport models by comparison with research aircraft observations. Part 1: Concepts and overall model performance, Atmos. Chem. Phys., 3, 1609–1631, 2003, SRef-ID: 1680-7324/acp/2003-3-1609. 3058, 3075

Brunner, D., Staehelin, J., Rogers, H. L., et al.: An evaluation of the performance of chemistry transport models by comparison with research aircraft observations. Part 2: Detailed comparison with two selected campaigns, Atmos. Chem. Phys., 5, 107–129, 2005, SRef-ID: 1680-7324/acp/2005-5-107. 3058, 3075, 3076

Choi, Y., Wang, Y., Zeng, T., Martin, R. V., Kurosu, T. P., and Chance, K.: Evidence of lightning NO_x and convective transport of pollutants in satellite observations over North America, Geophys. Res. Lett., 32, L02805, doi:10.1029/2004GL021436, 2005. 3050

Christian, H. J., Blakeslee, R. J., Boccippio, D. J., et al.: Global frequency and distribution of lightning as observed from space by the Optical Transient Detector, J. Geophys. Res., 108(D1), 4005, doi:10.1029/2002JD002347, 2003. 3056

Crutzen, P. J.: The influence of nitrogen oxides on atmospheric ozone content, Q. J. R. Meteorol. Soc., 97, 320–325, 1970. 3049

Dentener, F., van Weele, M., Krol, M., Houweling, S., and van Velthoven, P.: Trends and interannual variability of methane emissions derived from 1979–1993 global CTM simulations, Atmos. Chem. Phys., 3, 73–88, 2003, SRef-ID: 1680-7324/acp/2003-3-73. 3053

Duncan, B. N., Martin, R. V., Staudt, A. C., Yevich, R., and Logan, J. A.: Interannual and seasonal variability of biomass burning emissions constrained by satellite observations, J. Geophys. Res., 108, 4100, doi:10.1029/2002JD002378, 2003. 3065

Elvidge, C. D., Imhoff, M. L., Baugh, K. E., Hobson, V. R., Nelson, I., Safran, J., Dietz, J. B., and Tuttle, B. T.: Nighttime Lights of the World: 1994–95, ISPRS Journal of Photogrammetry and Remote Sensing, 56, 81–99, 2001. 3061

Emmonds, L. K., Carroll, M. A., Hauglustaine, D. A., et al.: Climatologies of NO_x and NO_y: a comparison of data and models, Atmos. Environ., 31, 1851–1904, 1997. 3075

Eskes, H. J. and Boersma, K. F.: Averaging kernels for DOAS total-column satellite retrievals, Atmos. Chem. Phys., 3, 1285–1291, 2003, SRef-ID: 1680-7324/acp/2003-3-1285. 3052, 3053, 3060

Feigelson, E. M.: Radiation in a cloudy atmosphere, D. Riedel Publishing Company, Dordrecht, 1984. 3056

Gallardo, L. and Cooray, V.: Could cloud-to-cloud discharges be as effective as cloud-to-ground discharges in producing NO_x?, Tellus, 48B, 641–651, 1996. 3067

Hild, L., Richter, A., Rozanov, V., and Burrows, J. P.: Air mass facto calculations for GOME measurements of lightning-produced NO_2, Adv. Space Res., 29, 11, 1685–1690, 2002. 3050, 3054, 3056

Huntrieser, H., Schlager, H., Feigl, C., and Höller, H.: Transport and production of NO_x in electrified thunderstorms: Survey of previous studies and new observations at midlatitudes, J. Geophys. Res., 103, 28 247–28 264, 1998. 3065, 3088

Huntrieser, H., Feigl, C., Schlager, H., Schröder, F., Gerbig, C., van Velthoven, P., Flatoy, F., Thery, C., Petzold, A., Höller, H., and Schumann, U.: Airborne measurements of NO_x, tracer species, and small particles during the European Lightning Nitrogen Oxides Experiment, J. Geophys. Res., 107(D11), doi:10.1029/2000JD000209, 2002. 3088

Jaeglé, L., Martin, R. V., Chance, K., Steinberger, L., Kurosu, T. P., Jacob, D. J., Modi, A. I., Yoboué, V., Sigha-Nkamdjou, L., and Galy-Lacaux, C.: Satellite mapping of rain-induced nitric oxide emissions from soils, J. Geophys. Res., 109, D21310, doi:10.1029/2004JD004787, 2004. 3065

Jourdain, L. and Hauglustaine, D. A.: The global distribution of lightning NO_x simulated on-line in a general circulation model, Phys. Chem. Earth (C), 26, 585–591, 2001. 3067, 3075

Koelemeijer, R. B. A., Stammes, P., Hovenier, J. W., and De Haan, J. F.: A fast method for retrieval of cloud parameters using oxygen A band measurements from the Global Ozone Monitoring Experiment, J. Geophys. Res., 106, 3475–3490, 2001. 3050, 3051, 3052

Kunhikrishnan, T., Lawrence, M. G., von Kuhlmann, R., Richter, A., Ladstätter-Weissenmayer, A., and Burrows, J. P.: Semiannual NO_2 plumes during the monsoon transition periods over the central Indian Ocean, Geophys. Res. Lett., 31, L08110, doi:10.1029/2003GL019269, 2004. 3068

Kurz, C. and Grewe, V.: Lightning and thunderstorms, Part I: Observational data and model results, Meteorologische Zeitschrift, 11, 379–393, doi:10.1127/0941-2948/2002/0011-0379, 2002. 3067, 3075, 3081

Labrador, L. J., von Kuhlmann, R., and Lawrence, M. G.: Strong sensitivity of the global mean OH concentration and the tropospheric oxidizing capacity to the source of NO_x from lightning, Geophys. Res. Lett., 31, L06102, doi:10.1029/2003GL019229, 2004. 3049

Labrador, L. J., von Kuhlmann, R., and Lawrence, M. G.: The effects of lightning-produced NO_x and its vertical distribution on atmospheric chemistry: sensitivity simulations with MATCH-

MPIC, Atmos. Chem. Phys. Discuss., 4, 6239–6281, 2004, SRef-ID: 1680-7375/acpd/2004-4-6239. 3076

Lee, D. S., Köhler, I., Grobler, E., Rohrer, F., Sausen, R., Gallardo-Klenner, L., Olivier, J. G. J., Dentener, F. J., and Bouwman, A. F.: Estimations of global NO_x emissions and their uncertainties, Atmos. Environ., 31, 1735–1749, 1997. 3059

Leue, C., Wenig, M., Wagner, T., Klimm, O., Platt, U., and Jähne, B.: Quantitative analysis of NO_x emissions from Global Ozone Monitoring Experiment satellite image sequences, J. Geophys. Res., 106, 5493–5505, 2001. 3049

Levy II, H., Moxim, W. J., and Kasibhatla, P. S.: J. Geophys. Res., 101(D17), 22 911–22 922, 1996. 3049, 3050, 3056, 3059, 3060, 3088

Martin, R. V., Chance, K., Jacob, D. J., Kurosu, T. P., Spurr, R. J. D., Bucsela, E., Gleason, J. F., Palmer, P. I., Bey, I., Fiori, A. M., Li, Q., Yantosca, R. M., and Koelemeijer, R. B. A.: An improved retrieval of tropospheric nitrogen dioxide from GOME, J. Geophys. Res., 107(D20), 4437, doi:10.1029/2001JD001027, 2002. 3049, 3052

Martin, R. V., Parrish, D. D., Ryerson, T. B., Nicks Jr., D. K., Chance, K., Kurosu, T. P., Jacob, D. J., Sturges, E. D., Fried, A., and Wert, B. P.: Evaluation of GOME satellite measurements of tropospheric NO_2 and HCHO using regional data from aircraft campaigns in the southeastern United States, J. Geophys. Res., 109(D24), D24307, doi:10.1029/2004JD004869, 2004. 3052

McCollum, J. R., Gruber, A., and Ba, M. B.: Discrepancy between gauges and satellite estimates of rainfall in equatorial Africa, J. Appl. Meteorol., 39, 666–679, 2000. 3067

Meijer, E. W., van Velthoven, P. F. J., Thompson, A. M., Pfister, L., Schlager, H., Schulte, P., and Kelder, H. M.: Model calculations of the impact of NO_x from air traffic, lightning, and surface emissions, compared with measurements, J. Geophys. Res., 105, 3833–3850, 2000. 3058, 3075

Meijer, E. W., van Velthoven, P. F. J., Brunner, D., Huntrieser, H., and Kelder, H. M.: Improvement and evaluation for the parameterisation of nitrogen oxide production by lightning, Phys. Chem. Earth, 26, 577–583, 2001. 3058

Michalon, N., Nassif, A., Saouri, T., Royer, J. F., and Pontikis, C. A.: Contributionto the climatological study of lightning, Geophys. Res. Lett., 26, 3097–3100, 1999. 3056

Nesbitt, S. W., Zhang, R., and Orville, R. E.: Seasonal and global NO_x productionby lightning estimated from the Optical Transient Detector (OTD), Tellus, 52B, 1206–1215, 2000. 3049, 3088

Nesbitt, S. W. and Zipser, E. J.: The diurnal cycle of rainfall and convective intensity according to Three years of TRMM measurements, J. Climate, 16, 1456–1475, 2002. 3057

Olivier, J. G. J. and Berdowsky, J. J. M.: Global emission sources and sinks, in: The Climate System, edited by: Berdowski, J., Guicherit, R., and B. J. Heij, A. A. Balkema Publishers/Swets and Zeitlinger Publishers, Lisse, The Netherlands, 33–78, ISBN 90 5809 255 0, 2001. 3049

Pickering, K. E., Wang, Y., Tao, W.-K., Price, C., and Müller, J.-F.: Vertical distributions of lightning NO_x for use in regional and global chemical transport models, J. Geophys. Res., 103, 31 203–31 216, 1998. 3053, 3059

Price, C. and Rind, D.: A Simple Lightning Parameterization for Calculating Global Lightning Distributions, J. Geophys. Res., 97(D9), 9919–9933, 1992. 3054, 3056, 3058, 3080

Price, C. and Rind, D.: What determines the cloud-to-ground lightning fraction in thunderstorms?, Geophys. Res. Lett., 20, 463–466, 1993. 3059

Price, C., Penner, J., and Prather, M.: NO_x from lightning – 1. Global distribution based on lightning physics, J. Geophys. Res., 102, 5929–5941, 1997a. 3049, 3059, 3088

Price, C., Penner, J., and Prather, M.: NO_x from lightning – 2. Constraints from the global atmospheric circuit, J. Geophys. Res., 102, 5943–5951, 1997b. 3088

Richter, A. and Burrows, J. P.: Tropospheric NO_2 from GOME measurements, Adv. Space Res., 29, 1673–1683, 2002. 3049

Ridley, B. A., Walega, J. G., Dye, J. E., and Grahek, F. E.: Distributions of NO, NO_x, NO_y, O_3 to 12 km altitude during the summer monsoon season over New Mexico, J. Geophys. Res., 99, 25 519–25 534, 1994. 3053

Ridley, B. A., Dye, J. E., Walega, J. G., Zheng, J., Grahek, F. E., and Rison, W.: On the production of active nitrogen by thunderstorms over New Mexico, J. Geophys. Res., 101(D15), 20 985–21 005, 1996. 3054, 3088

Ushio, T., Heckman, S. J., Boccippio, D. J., and Christian, H. J.: A survey of thunderstorm flash rates compared to cloud top height using TRMM satellite data, J. Geophys. Res, 106(D20), 24 089–24 095, 2001. 3054, 3056, 3059, 3067

Wagner, T., Leue, C., Wenig, M., and Platt, U.: GOME NO_2 validation studies, in: ERS-2 GOME Data Products Delta Characterisation Report 1999, edited by: Lambert, J.-C. and Skarlas, P., Frascati, 87–96, 1999. 3051

Wang, Y., DeSilva, A. W., Goldenbaum, G. C., and Dickerson, R. R.: Nitric oxide production by simulated lightning: Dependence on current, energy, and pressure, J. Geophys. Res.,

103(D15), 19 149–19 159, 1998. 3088
Wauben, W. M. F., van Velthoven, P. F. J., and Kelder, H. M.: A 3D chemistry transport model study of changes in atmospheric ozone due to aircraft NO_x emissions, Atmos. Environ., 31, 1819–1836, 1997. 3075
Wenig, M., Huehl, S. Beirle, S., Bucsela, E., Jähne, B., Platt, U., Gleason, J., and Wagner, T.: Retrieval and analysis of stratospheric NO_2 from the Global Ozone Monitoring Experiment, J. Geophys. Res., 109, D04315, doi:10.1029/2003JD003652, 2004. 3051
Yienger, J. J. and Levy II, H.: Empirical model of global soil-biogenic NO_x emissions, J. Geophys. Res., 100(D6), 11 447–11 464, 1995. 3065

Table 1. Overview of recently published estimates of global annual lightning NO_x production. P denotes the estimated production of LNO_x in $TgNyr^{-1}$.

Study	P	Range	Method
Levy et al. (1996)	4.0	3.0 – 5.0	Top-down from aircraft NO_x observations
Ridley et al. (1996)	n.a	2.0 – 5.0	Extrapolation of New Mexico storm production
Price et al. (1997a)	12.2	5.0 – 20.0	Bottom-up from ISCCP cloud climatology
Price et al. (1997b)	13.2	5.0 – 25.0	Constraints from atmospheric electricity
Wang et al. (1998)	n.a	2.5 – 8.3	Bottom-up from laboratory measurements
Huntrieser et al. (1998)	4.0	0.3 – 22.0	Extrapolation of LINOX storm production
Nesbitt et al. (2000)	n.a	0.9 – 8.8	Bottom-up from OTD flash climatology
Huntrieser et al. (2002)	3.0	1.0 – 20.0	Extrapolation of EULINOX storm production
Allen and Pickering (2002)	n.a	1.7 – 12.2	Bottom-up from validated model flash rates
Beirle et al. (2004)	2.8	0.8 – 14.0	Top-down from satellite observations over Australia

Table 2. TM3 grid cell acceptance criteria based on OLS nighttime lights climatology. The relative intensity applies to the average (binned) relative light intensity in a 2.5°×2.5° TM3 grid cell.

Relative intensity	Decision
<4%	Accept grid cell
4–8%	Reject grid cell
8–20%	Reject grid cell and 8 surrounding grid cells (3×3)
>20%	Reject grid cell, 8 surrounding, and 3 adjacent East and West grid cells (3×5)

Table 3. TM3 grid cell acceptance criteria based on monthly ATSR fire counts maps. The relative intensity applies to the summed number of fires in a 2.5°×2.5° TM3 grid cell.

No. of fires in month	Decision
0	Accept grid cell
<50	Reject grid cell and 8 surrounding grid cells (3×3)
50–100	Reject grid cell and 8 surrounding grid cells, and 3 adjacent East and West grid cells (3×5)
>100	Reject grid cell, 8 surrounding, and 2×3 adjacent East and West grid cells (3×7)

Table 4. Slope corrections ($s_{sim}-1$) from TM3 LNO2 vs. TM3 total NO_2 analyses. These numbers were computed with the temporal and spatial correlation method for grid cells with cloud-free observations.

	CP		H5	
Area	Temporal	Spatial	Temporal	Spatial
Pacific Ocean	0.19	0.22	0.33	0.38
South America	0.08	0.08	0.21	0.21
Atlantic Ocean	0.09	0.23	0.23	0.26
Africa	0.13	0.31	0.15	0.20
Indian Ocean	0.36	0.35	0.43	0.41
Australia	0.23	0.46	0.18	0.41

Table 5. Results from 8 methods to estimate the global LNOx production. The column headed 'World' includes the random error estimate. The column headed 'Total error' combines the random and systematic contributions to the error estimate.

Scheme	Method	Observation type	World	Total error	40° S–5° N
CP	Temporal	Clear sky	3.2±0.8	1.4	1.1±0.2
CP	Spatial	Clear sky	2.7±0.7	1.2	1.0±0.2
CP	Temporal	Cloudy sky	2.3±0.9	1.2	0.9±0.2
CP	Spatial	Cloudy sky	2.8±0.8	1.3	1.3±0.2
H5	Temporal	Clear sky	4.6±0.8	1.8	1.0±0.1
H5	Spatial	Clear sky	4.5±0.8	1.8	1.1±0.1
H5	Temporal	Cloudy sky	3.9±1.5	2.0	1.0±0.1
H5	Spatial	Cloudy sky	4.0±1.2	1.8	1.4±0.1
		Average:	3.5±0.9	1.6	1.1

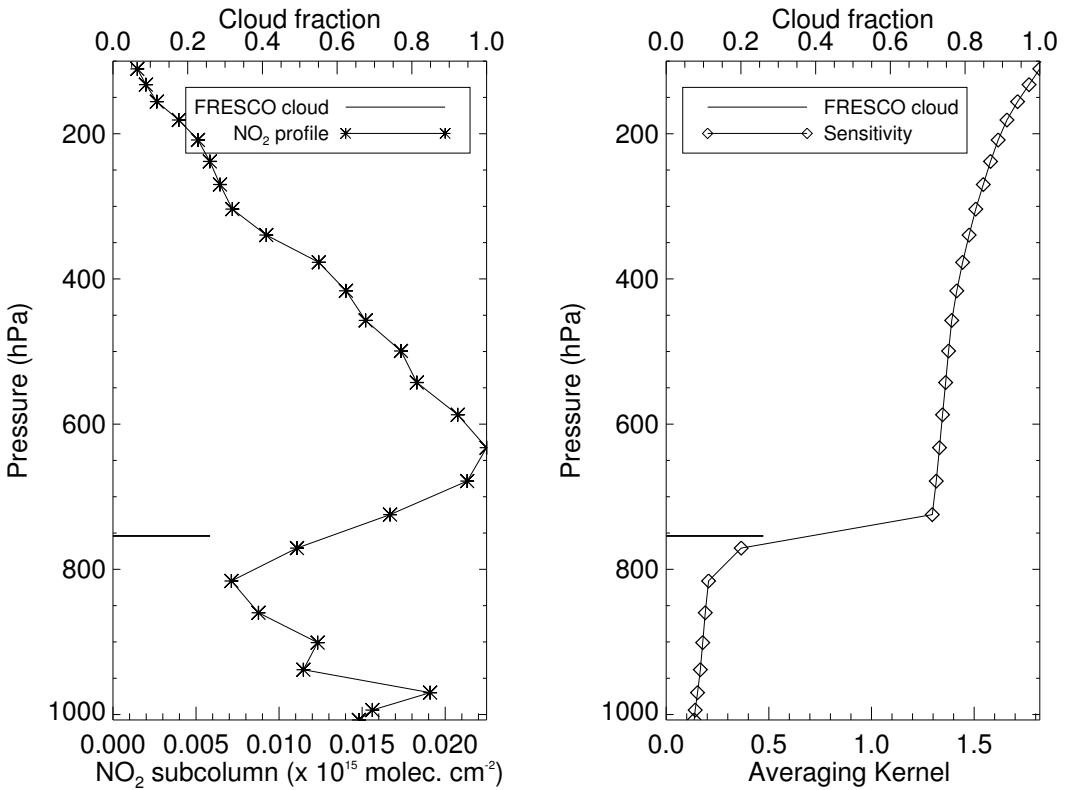

Fig. 1. Example of a GOME pixel with a low cloud over the Atlantic Ocean West of Angola (14.64° S, 2.7° E) on 5 January 1997. The left panel shows the predicted TM3 NO_2 tropospheric profile and FRESCO cloud parameters. The right panel shows the corresponding averaging kernel.

ACPD
5, 3047–3104, 2005

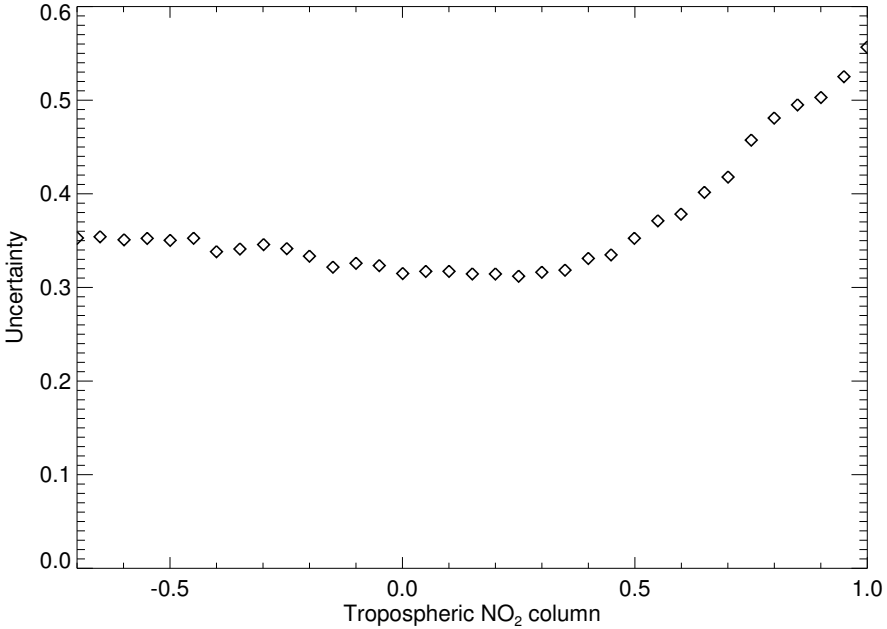

Fig. 2. Average tropospheric NO_2 column retrieval error as a function of column value (both in 10^{15} molec.cm^{-2}). Average calculated for the month of January 1997 for pixels in the 40° S–5° N region.

ACPD
5, 3047–3104, 2005

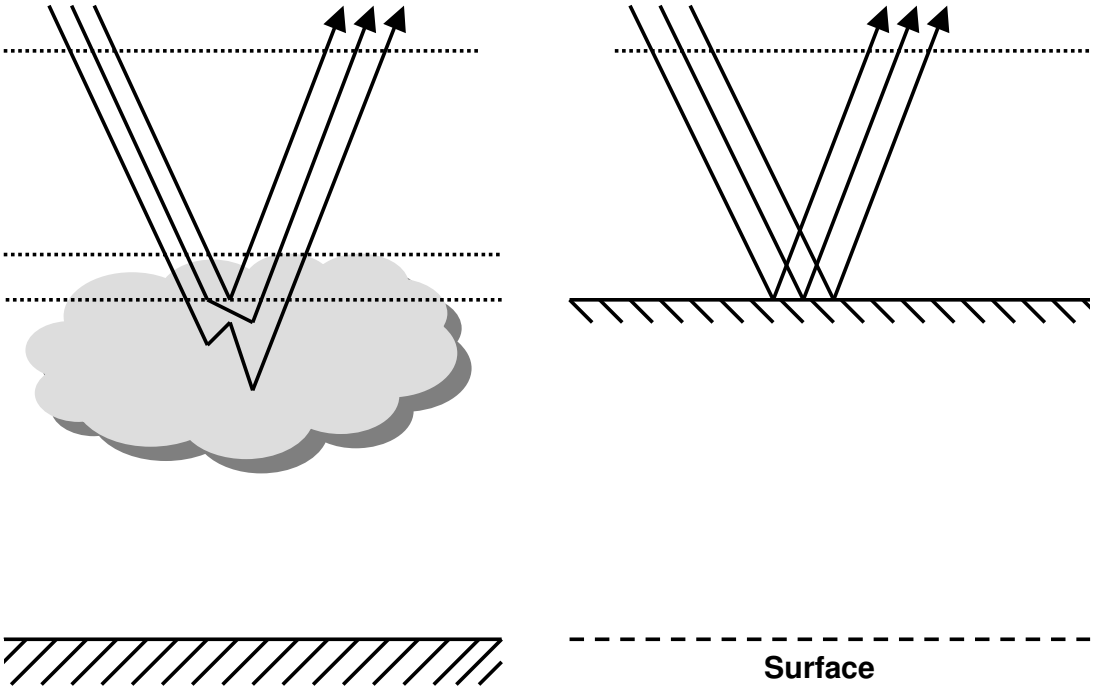

Fig. 3. Schematic illustration of photons sampling the upper part of a cloud (left) and how this process is modelled in FRESCO and NO_2 air mass factor calculations (right).

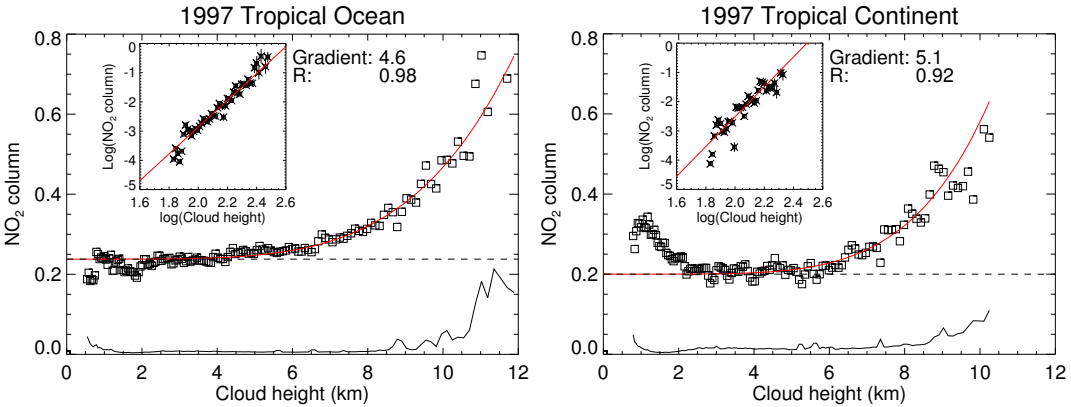

Fig. 4. The 1997-average of GOME observed near and above cloud top NO_2 column (unit 10^{15} molecules cm^{-2}) as a function of the cloud top height retrieved from GOME data with the FRESCO algorithm. The red curves represent the power-law fits. The dashed lines estimate the background due to other NO_x sources. The bottom solid lines represent the standard deviations of the mean NO_2 column per cloud-top pressure bin of 5 hPa. The left panel shows the cloud top dependency for tropical oceans, and the right panel for tropical continents.

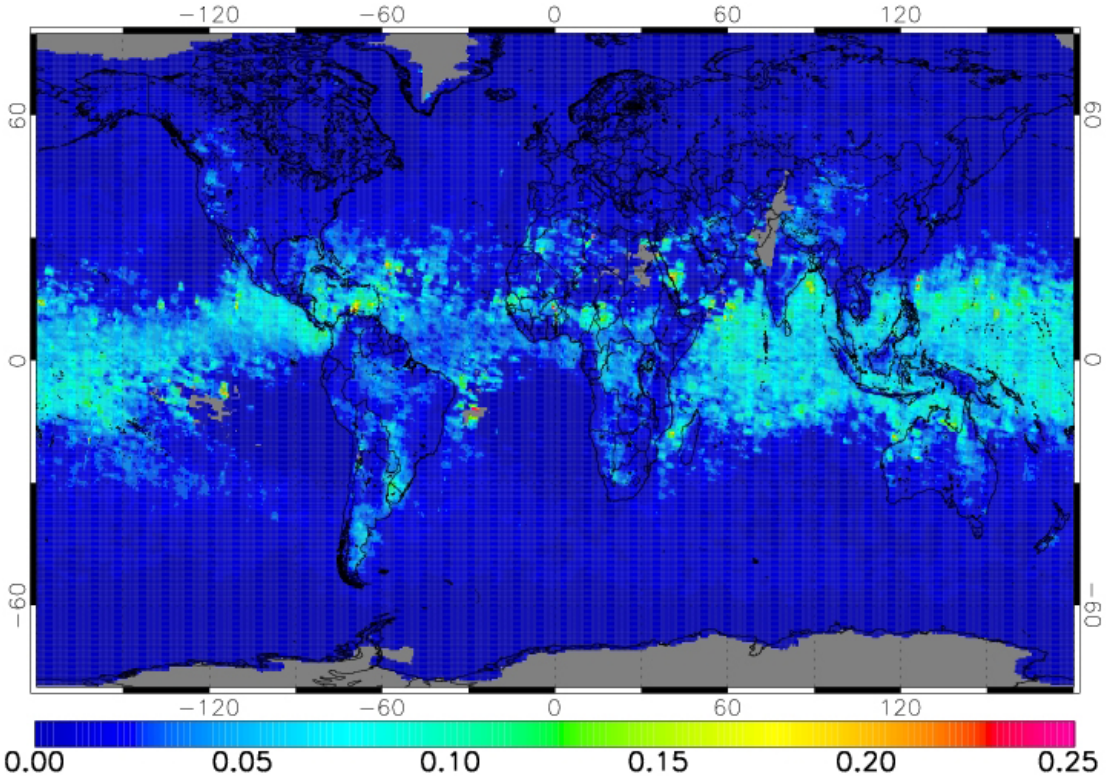

Fig. 5. The 1997 average of 10:30 hrs lightning-produced above and near cloud top NO_2 columns as derived from GOME. Produced columns in 10^{15} molec.cm^{-2}.

ACPD
5, 3047–3104, 2005

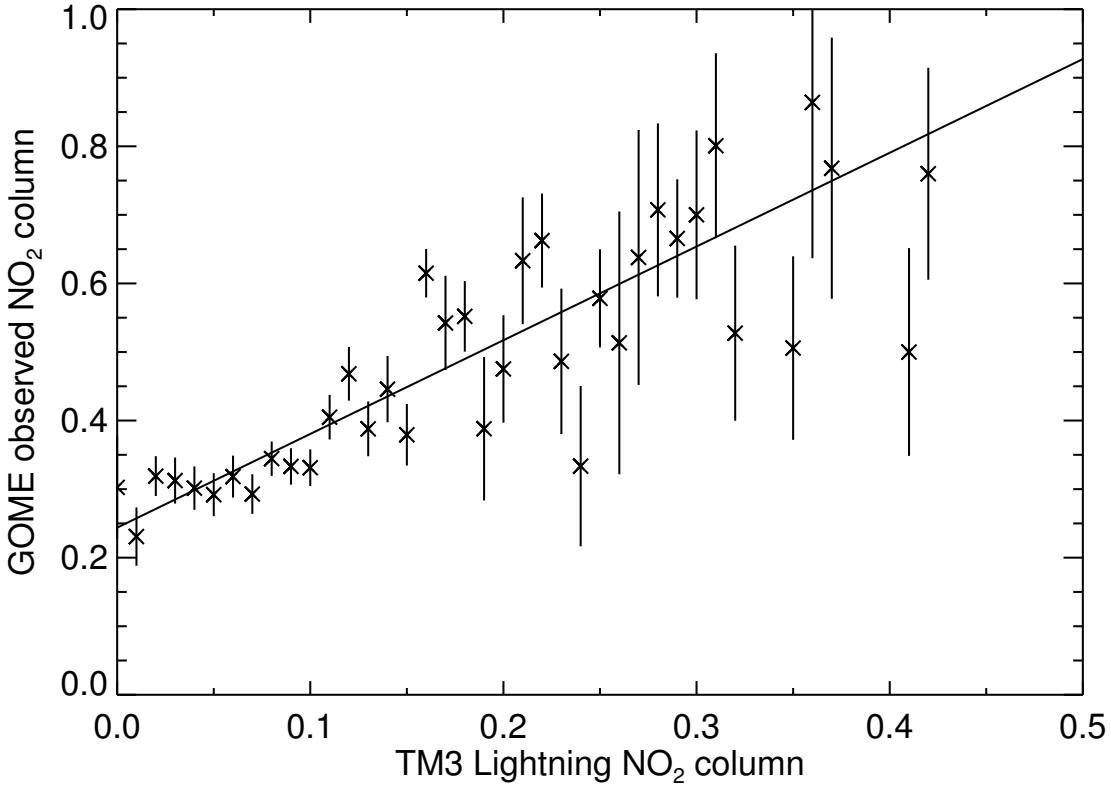

Fig. 6. GOME observed tropospheric NO2 as a function of the TM3 modelled LNO2 column, for the Australian region defined in Fig. 10. Shown is a 1997 average for scenes with small cloud fractions. Due to the masking of areas exposed to biomass burning the winter-spring period is sampled more often. Error bars correspond to the standard deviation of the mean of the observations in a given bin. The line represents an error-weighted linear fit.

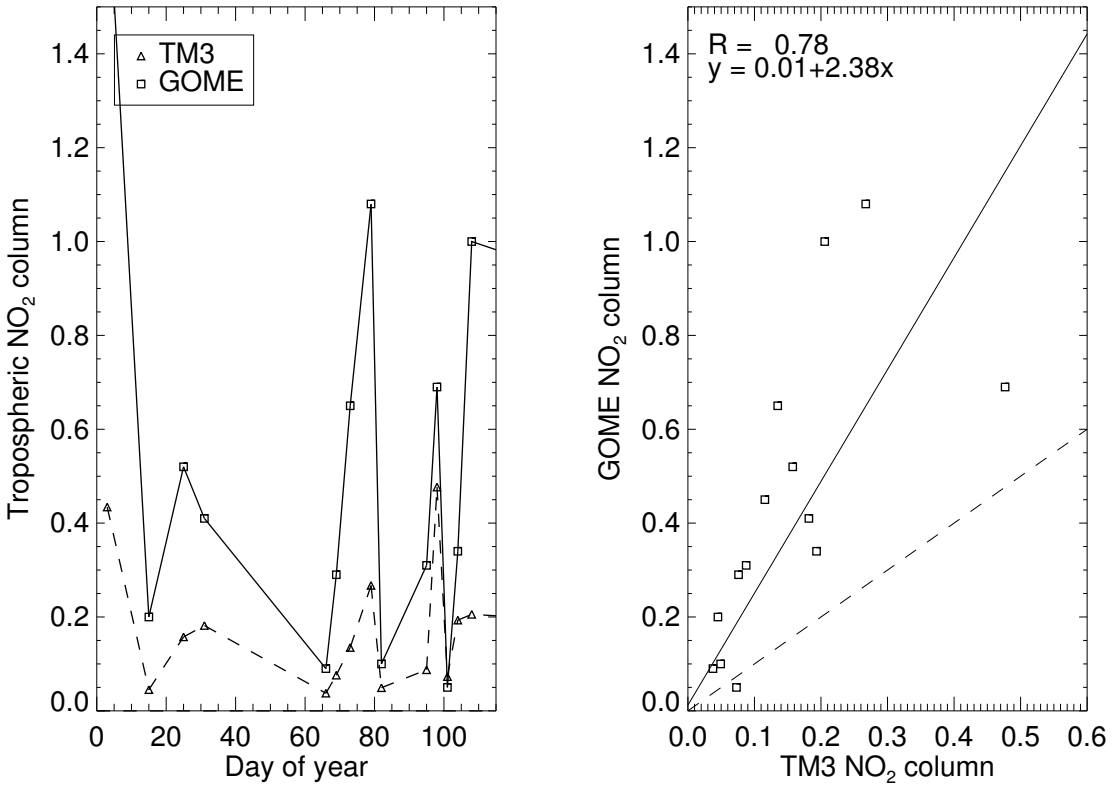

Fig. 7. An example of the temporal correlation method for a TM3 modelled LNO2 and GOME observed NO_2 column timeseries from 1 January to 1 May 1997, for the model grid cell at 18.75° S, 8.75° E (Congo, Africa).

ACPD
5, 3047–3104, 2005

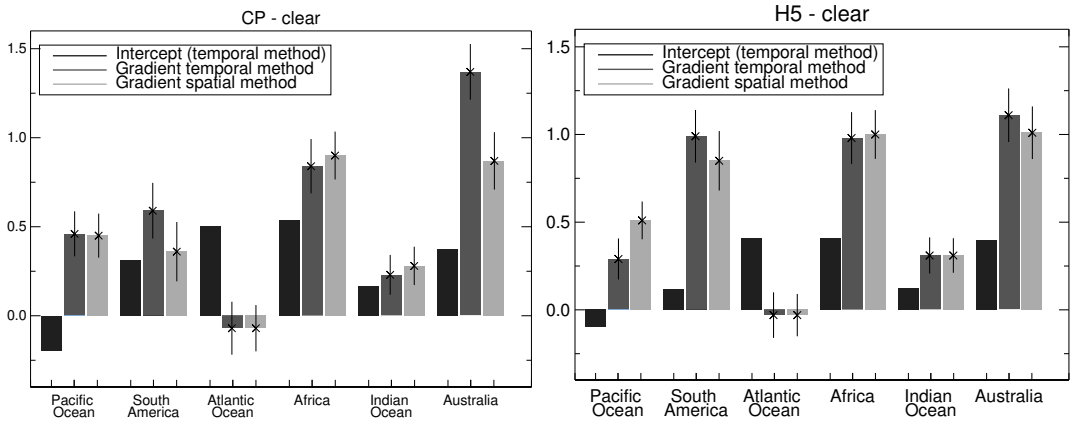

Fig. 8. Mean (corrected) slopes and intercepts of the GOME tropospheric NO2 columns as a function of TM3 LNO2, for the six regions shown in Fig. 10. GOME observations with small cloud reflectance fractions (<0.5) and modelled LNO2 columns based on the CP lightning scheme (left panel) and H5 scheme (right panel) are used. Dark grey: slopes for the temporal regression; light grey: slopes for the spatial regression; black: mean intercepts expressed as fraction of the absolute mean (temporal method). Error bars combine uncertainties of the mean regional slopes and the bias correction.

ACPD
5, 3047–3104, 2005

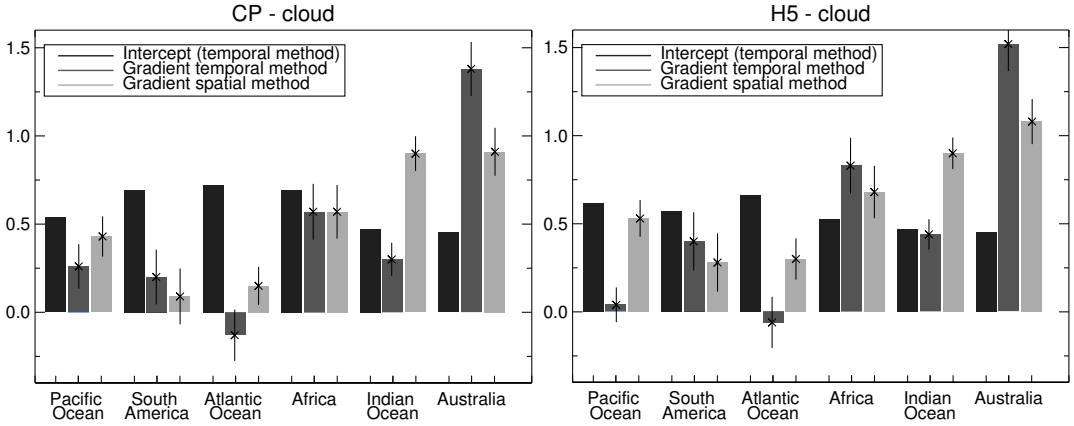

Fig. 9. As Fig. 8, but now for GOME observations with cloud reflectance fractions >0.5.

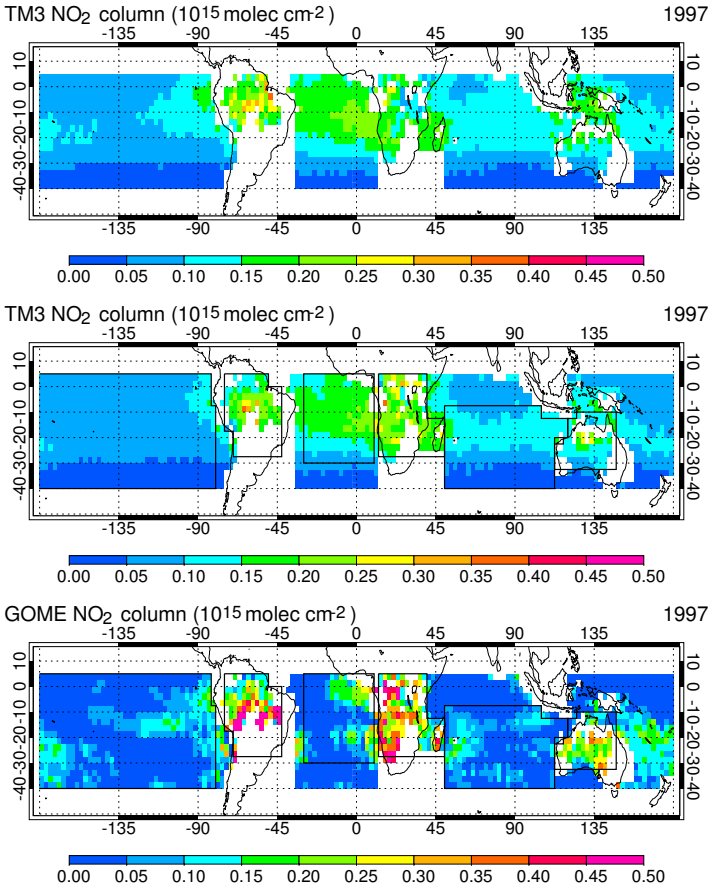

Fig. 10. Average (1997) lightning NO_2 column as modelled with the CP scheme (top panel), modelled with the H5 scheme (middle panel), and observed by GOME (bottom panel) as a function on longitude and latitude. Columns in 10^{15} molec.cm^{-2}.

ACPD
5, 3047–3104, 2005

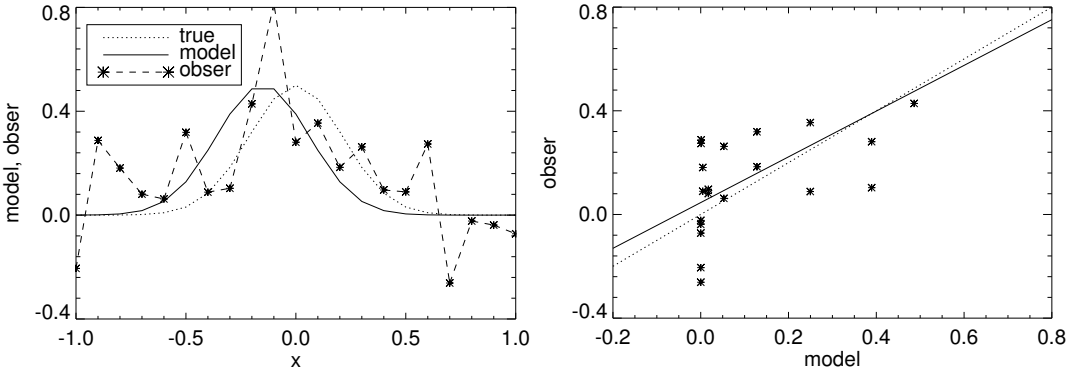

Fig. 11. Shift experiment. Upper panel: simulated observed and modelled patterns against arbitrary x-axis units (distance, time). Lower panel: corresponding regression analysis of observation vs. model (solid line). The dotted line indicates the regression line if there was no systematic error in the model and no noise on the observations.

ACPD
5, 3047–3104, 2005

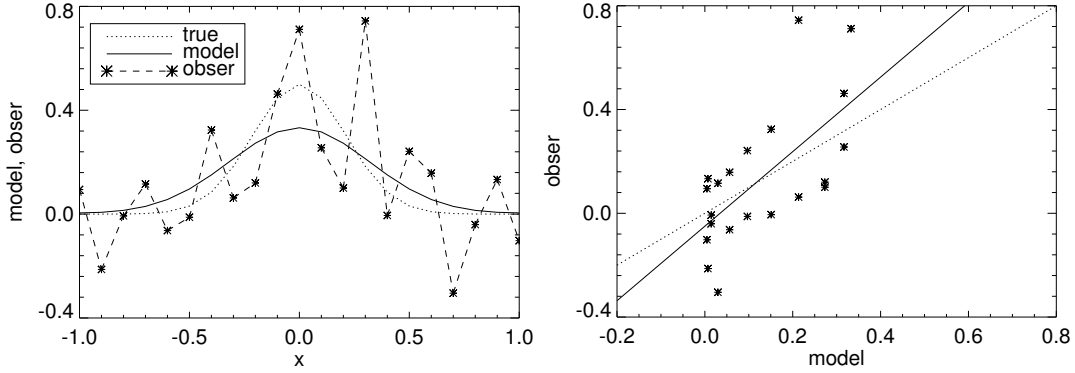

Fig. 12. Smearing experiment. Same as in Fig. 11, but now for a 'smeared' pattern.

ACPD
5, 3047–3104, 2005